# Microwave Remote Sensing of the Ocean

Dudley Chelton
Oregon State University

## *Overview:*

1. Why Microwave?
2. Brief overviews of the "Nuts and Bolts" of Microwave Remote Sensing:
   - Passive microwave radiometry
     *Radiometer measurements of SST, wind speed, water vapor, cloud liquid water, and salinity.*
   - Active radar systems
     *Radar altimeter measurements of sea surface height.*
     *Radar scatterometer measurements of ocean vector winds.*
3. Example Applications of Passive Microwave Radiometry
4. Example Applications of Altimetry
5. Example Applications of Scatterometry

# Definitions of Spectral Bands of Electromagnetic Radiation

**Table 3.3.** Naming conventions for radar bands of EMR
(1 GHz = $10^9$ Hz)

| Designation | Frequency range (GHz) | Center wavelength (cm) |
|---|---|---|
| P | 0.225 – 0.390 | 100 |
| L | 0.390 – 1.55 | 30 |
| S | 1.55 – 5.20 | 9 |
| C | 3.90 – 6.20 | 6 |
| X | 6.20 – 10.90 | 3.5 |
| $K_u$ | 10.90 – 18.00 | 2.1 |
| K | 18.00 – 26.00 | 1.4 |
| $K_a$ | 26.00 – 36.00 | 1.0 |
| Q | 36.00 – 46.00 | 0.7 |
| V | 46.00 – 56.00 | 0.6 |
| W | 56.00 – 100.00 | 0.4 |

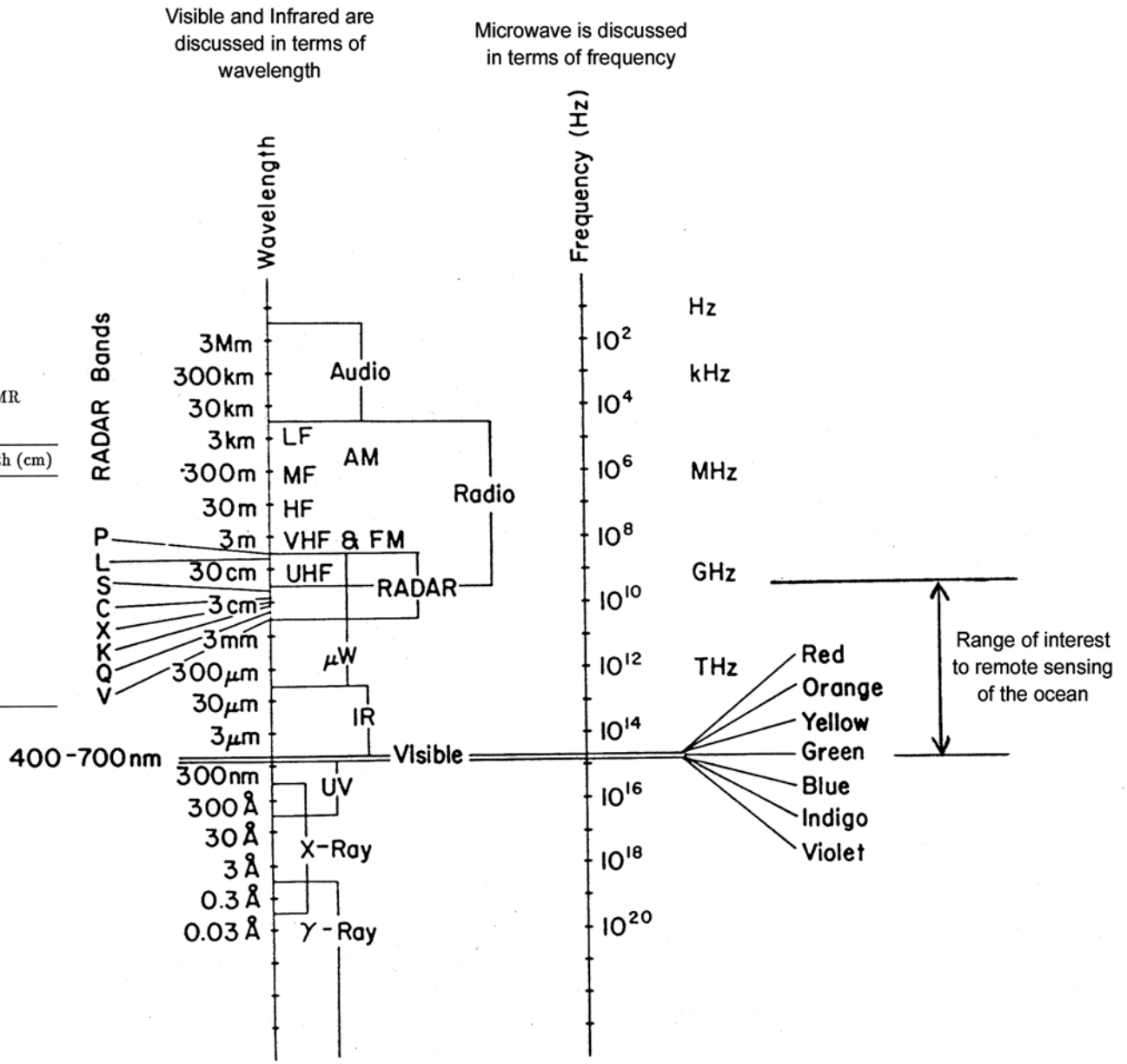

# Sources of EMR: Passive vs. Active Remote Sensing

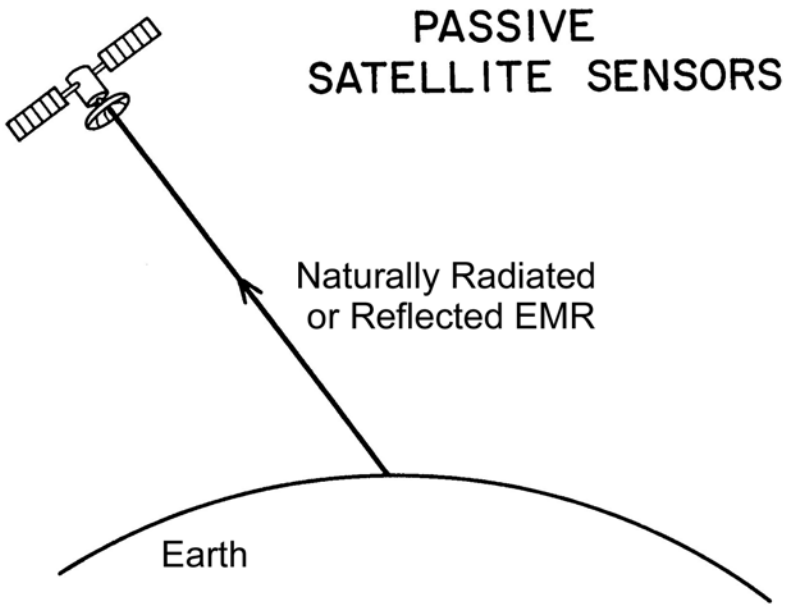


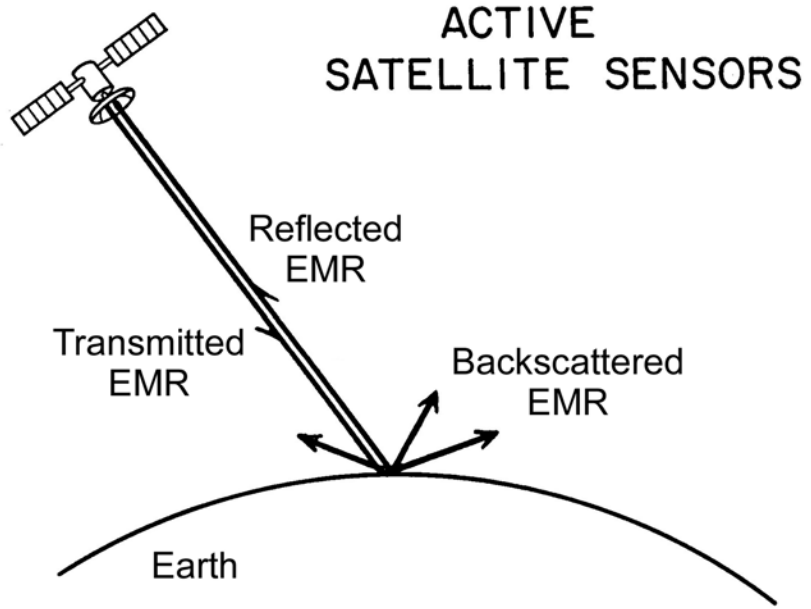


The source of natural radiation is thermal emission from molecular motion (heat), which varies with wavelength and depends on the surface roughness and the electrical properties of the emitting surface (conductivity, permittivity and permeability).

Active satellite sensors are radars that transmit microwave radiation toward the sea surface and measure the reflected (altimetry) or backscattered (scatterometry) signal.

## Microwave Sensors Most Relevant to Oceanography:

- *Passive Radiometer Measurements of Sea-Surface Temperature*
- *Radar Altimeter Measurements of Sea-Surface Height*
- *Radar Scatterometer Measurements of Surface Wind Stress*
- *Future:  Passive Radiometer Measurements of Sea-Surface Salinity*

# Why Microwave Remote Sensing?

#1: The primary reason is that clouds are nearly transparent to microwave EMR but opaque to Visible and Infrared EMR

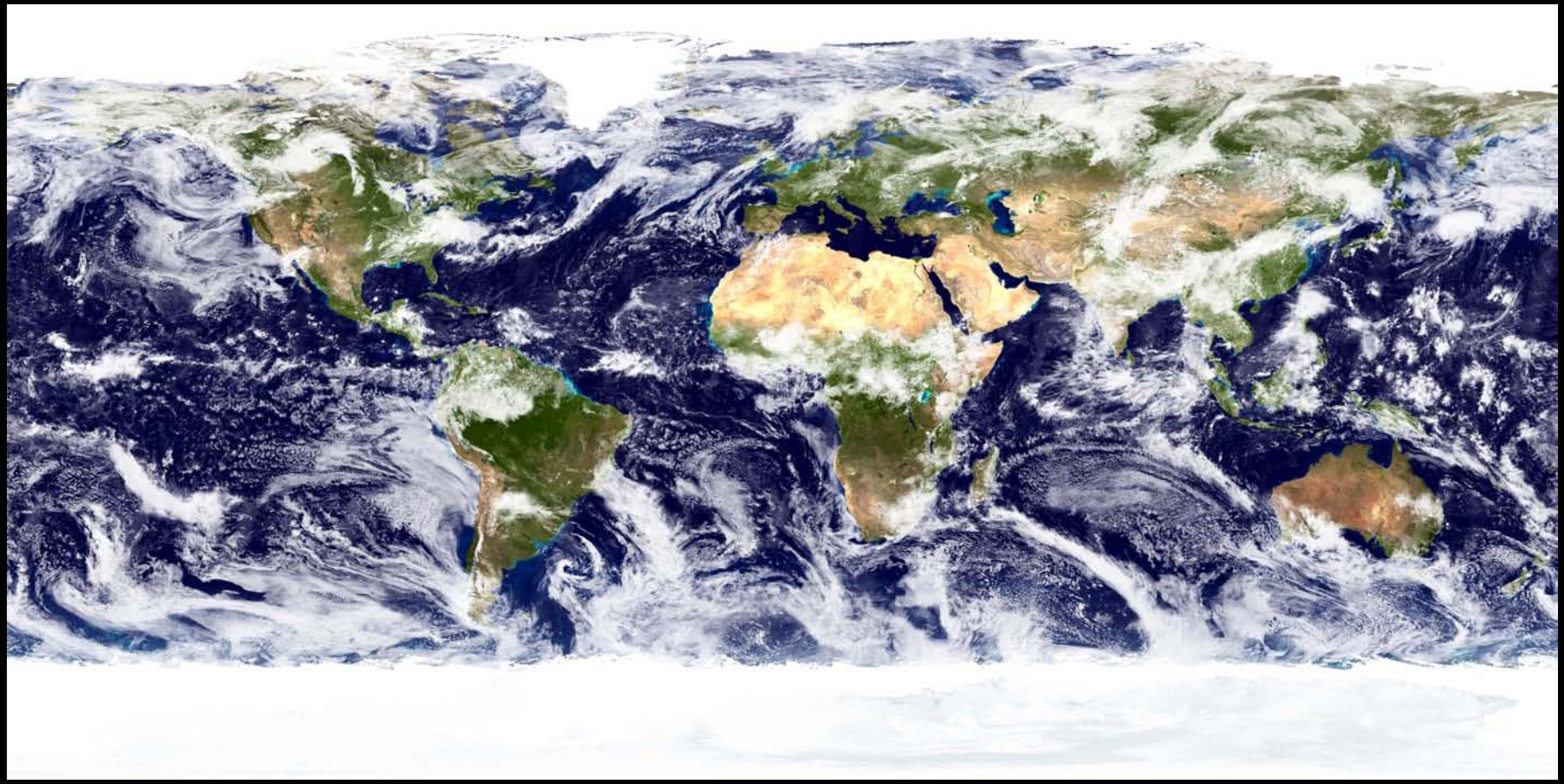

# Cloud Amount

ISCCP 2-Year Average

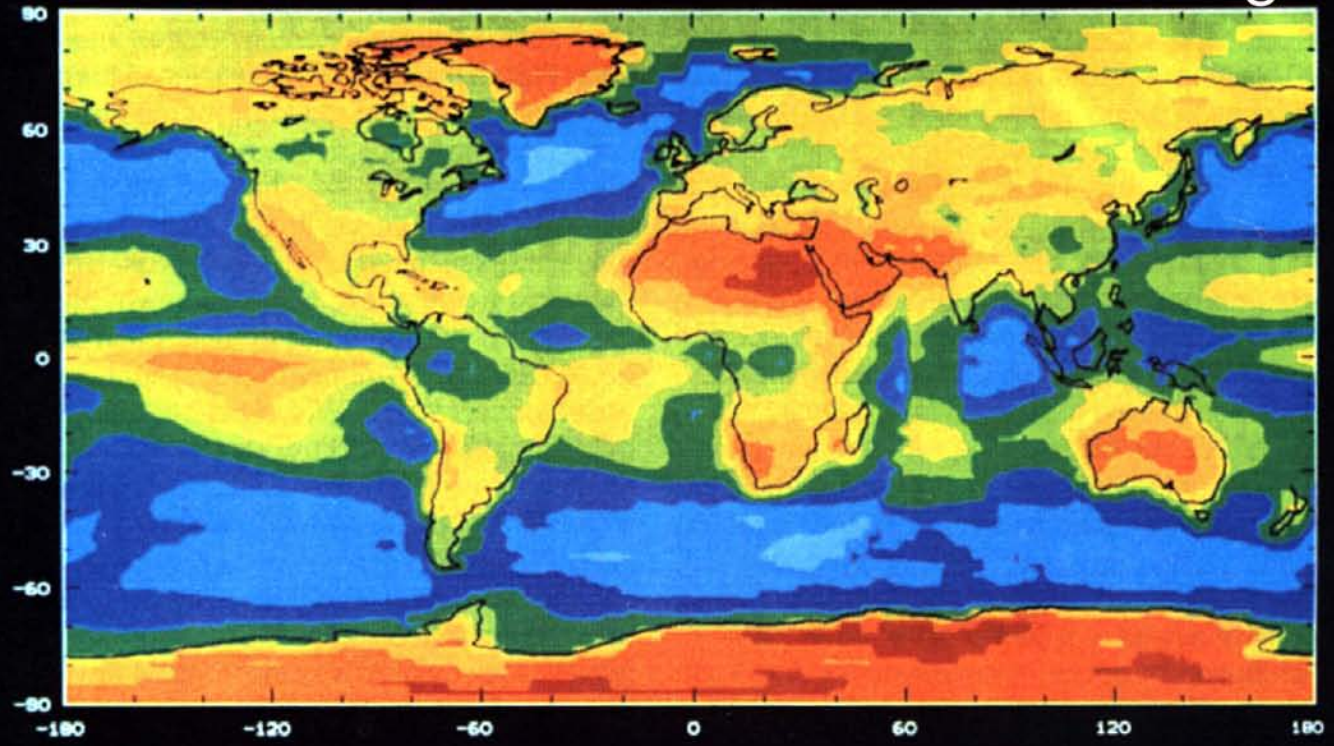


Global Monthly Mean = 59%


NASA/GISS
Rossow

# 2-Day Average Infrared Measurements of SST from the AVHRR (June 24-25, 2003)

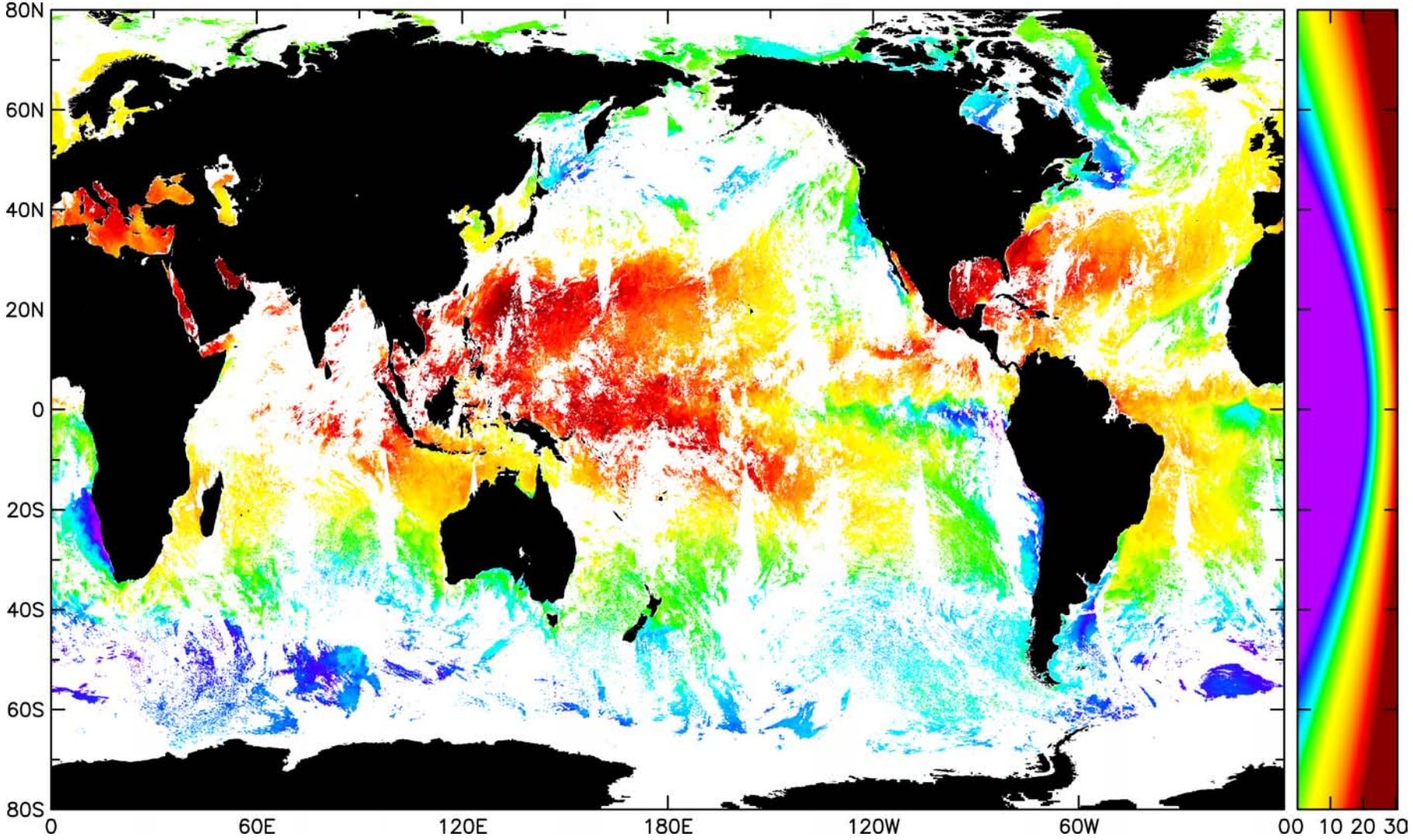

# 2-Day Average Microwave Measurements of SST from the AMSR (June 24-25, 2003)

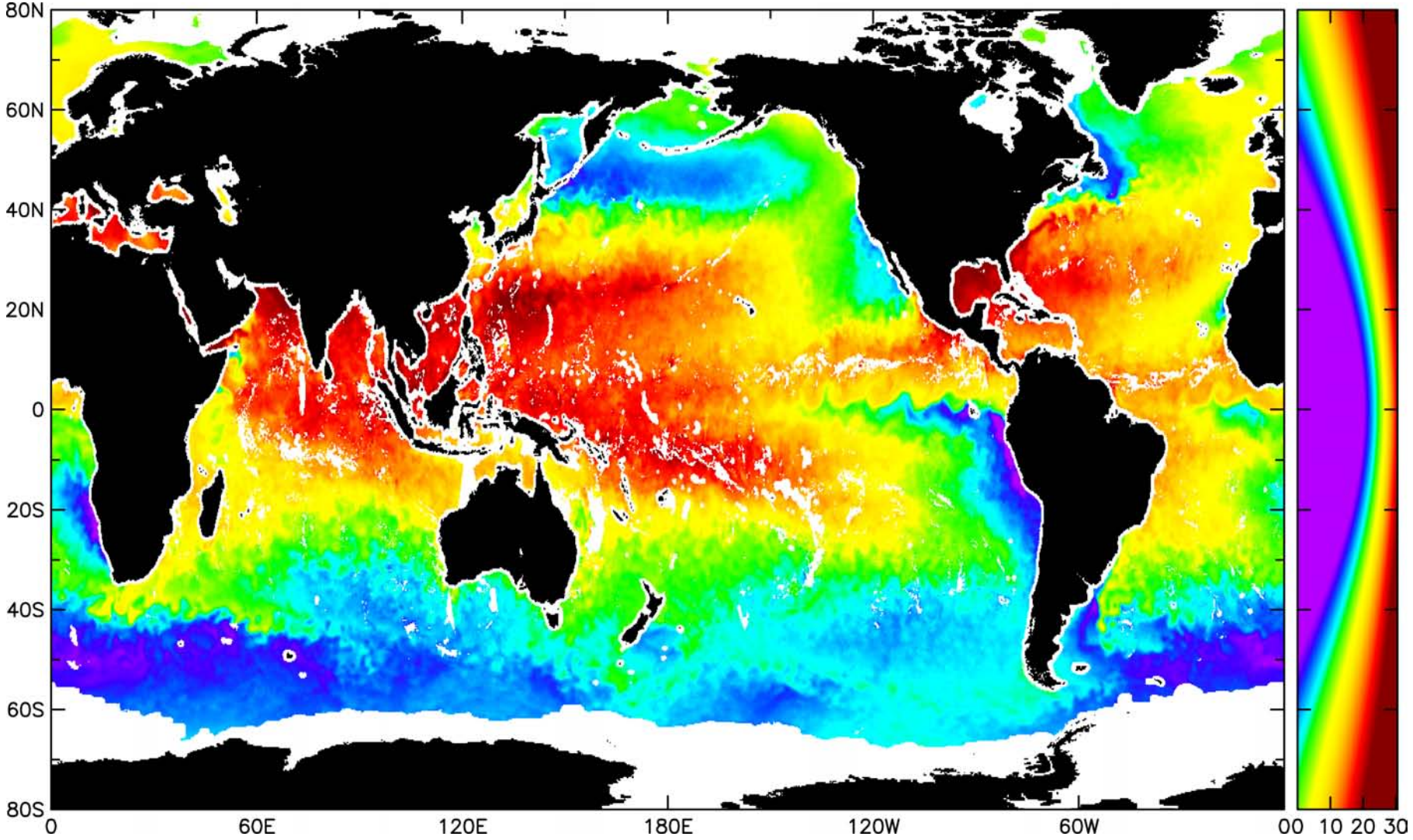

# #2: High Reflectance of the Sea Surface at Microwave Frequencies

(advantageous only to radar systems)

The reflectance is defined to be the ratio of the reflected spectral energy to the incident spectral energy, which depends on the wavelength (or, equivalently, the frequency) of the electromagnetic radiation.

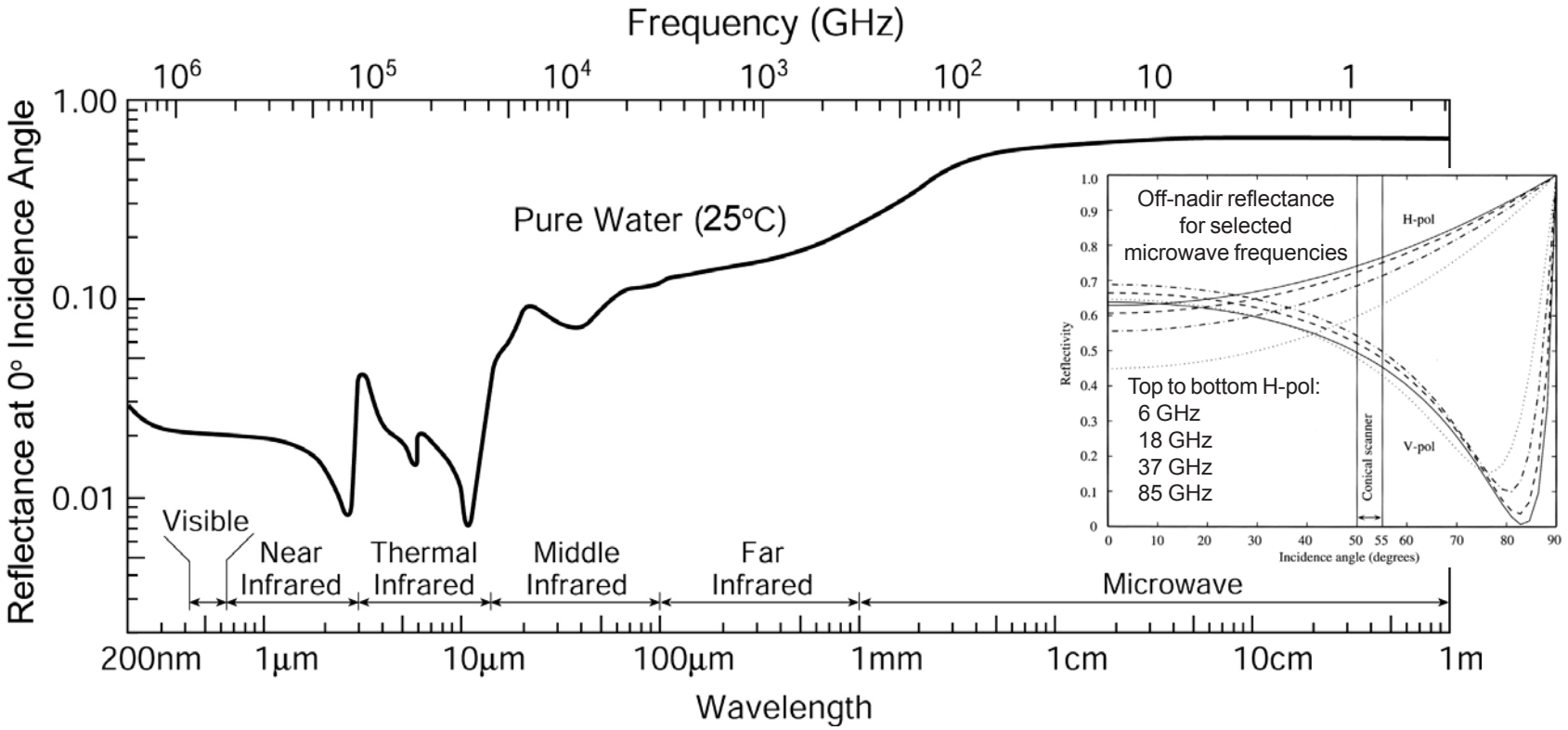


The reflectance at 0º incidence angle is less than 2% at visible and infrared wavelengths and exceeds 60% at microwave frequencies. At higher incidence angles, the reflectance increases for horizontally polarized electromagnetic raadiation and decreases for vertically polarized electromagnetic radiation (see inset).

The high reflectance of the sea surface at microwave frequencies yields a strong reflected signal for radar systems.

# #3: Weak Natural Emission at Microwave Frequencies

(advantageous only to radar systems)

Planck's Radiation Law for a perfect blackbody emitter:

Wavelength dependence (Visible and IR remote sensing)

$$L^{\lambda} = \frac{2hc_0^2}{\lambda^5} \frac{1}{e^{hc_0/(kT\lambda)} - 1} \quad W\,m^{-2}\,sr^{-1}\,\mu m^{-1}$$

Frequency dependence (Microwave remote sensing)

$$L^{f} = \frac{2hf^3}{c_0^2} \frac{1}{e^{hf/(kT)} - 1} \quad W\,m^{-2}\,sr^{-1}\,Hz^{-1}$$

$c_0 = 2.998 \times 10^8\ m\,s^{-1}$ speed of light in free space

$h = 6.63 \times 10^{-34}$ joule s Planck's constant

$k = 1.38 \times 10^{-23}$ joule $°K^{-1}$ Boltzman's constant

$T$ = absolute temperature in °K

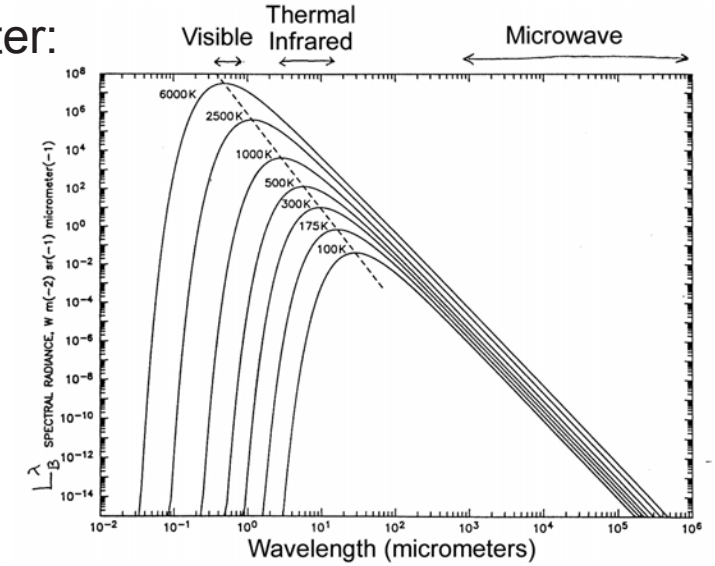


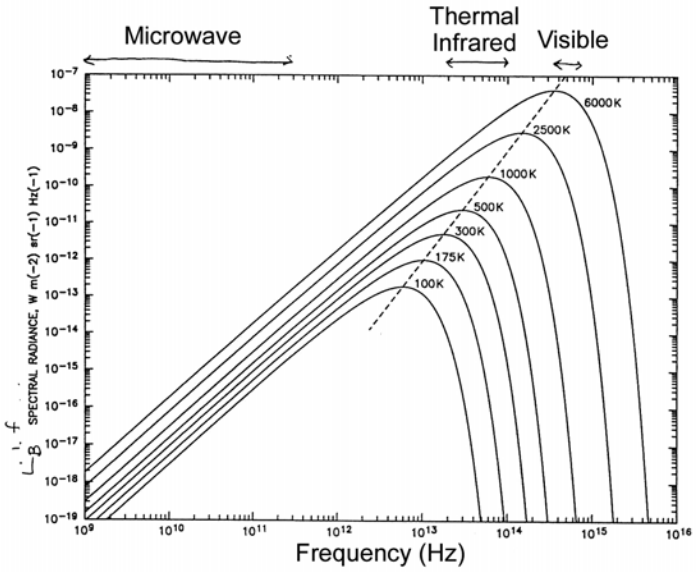


With increasing temperature T :

- The wavelength of maximum emission decreases
- The frequency of maximum emission increases

For a temperature of T = 300ºC, the ratio of the spectral radiance $L^f$ at a microwave frequency of 10 GHz to that at an infrared wavelength of 10 μm (i.e., a frequency of $3 \times 10^{13}$ Hz) is $2.78 \times 10^6$.

*At typical Earth temperatures, infrared emission is thus about a million times more energetic than microwave emission.*

# Rayleigh-Jeans Approximation of Planck's Law for Low Frequencies (Long Wavelengths)

Planck's Law: $L^f = \frac{2hf^3}{c_0^2} \frac{1}{e^{hf/(kT)} - 1}$

At the 1-50 GHz frequencies used in microwave remote sensing of the ocean, $hf/(kT) << 1$. At $f = 10$ GHz and $T = 300°K$, for example,

$$\frac{hf}{kT} = 1.6 \times 10^{-3}$$

The exponential in Planck's Law can therefore be approximated by a Taylor Series expansion:

$$e^x \approx 1 + x + \frac{x^2}{2} + \cdots$$

$$\approx 1 + x \quad \text{for} \quad x << 1$$

Substitution into Planck's Law yields

$$\boxed{L^f = \frac{2kf^2}{c_0^2} T}$$ Rayleigh-Jeans Approx.

Since $L^f$ and $T$ are linearly related at microwave frequencies, spectral radiance and blackbody temperature are often used interchangeably in microwave remote sensing.

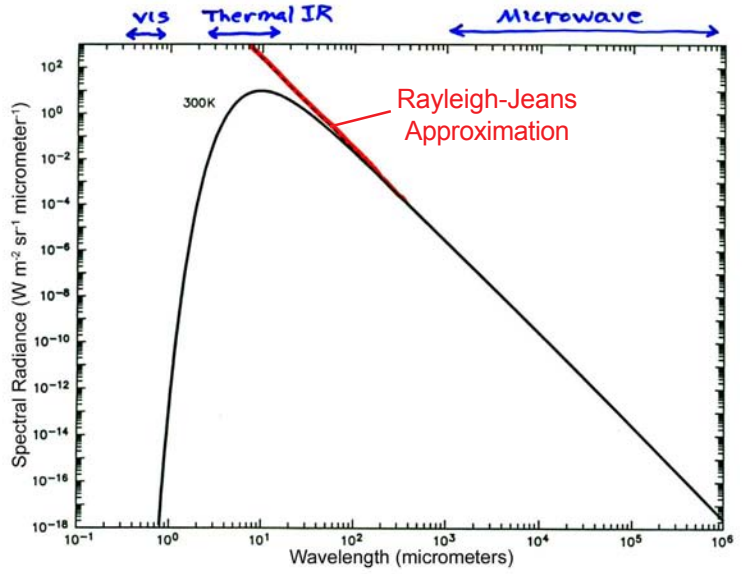


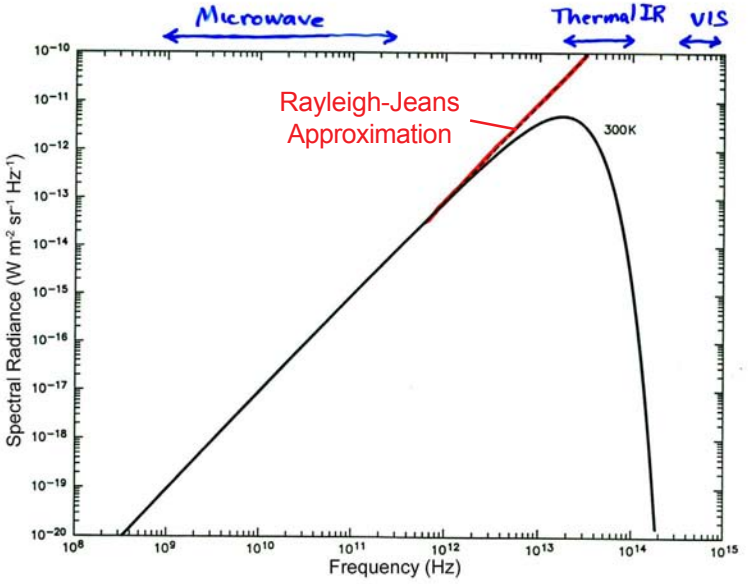

# Atmospheric Radiative Transfer

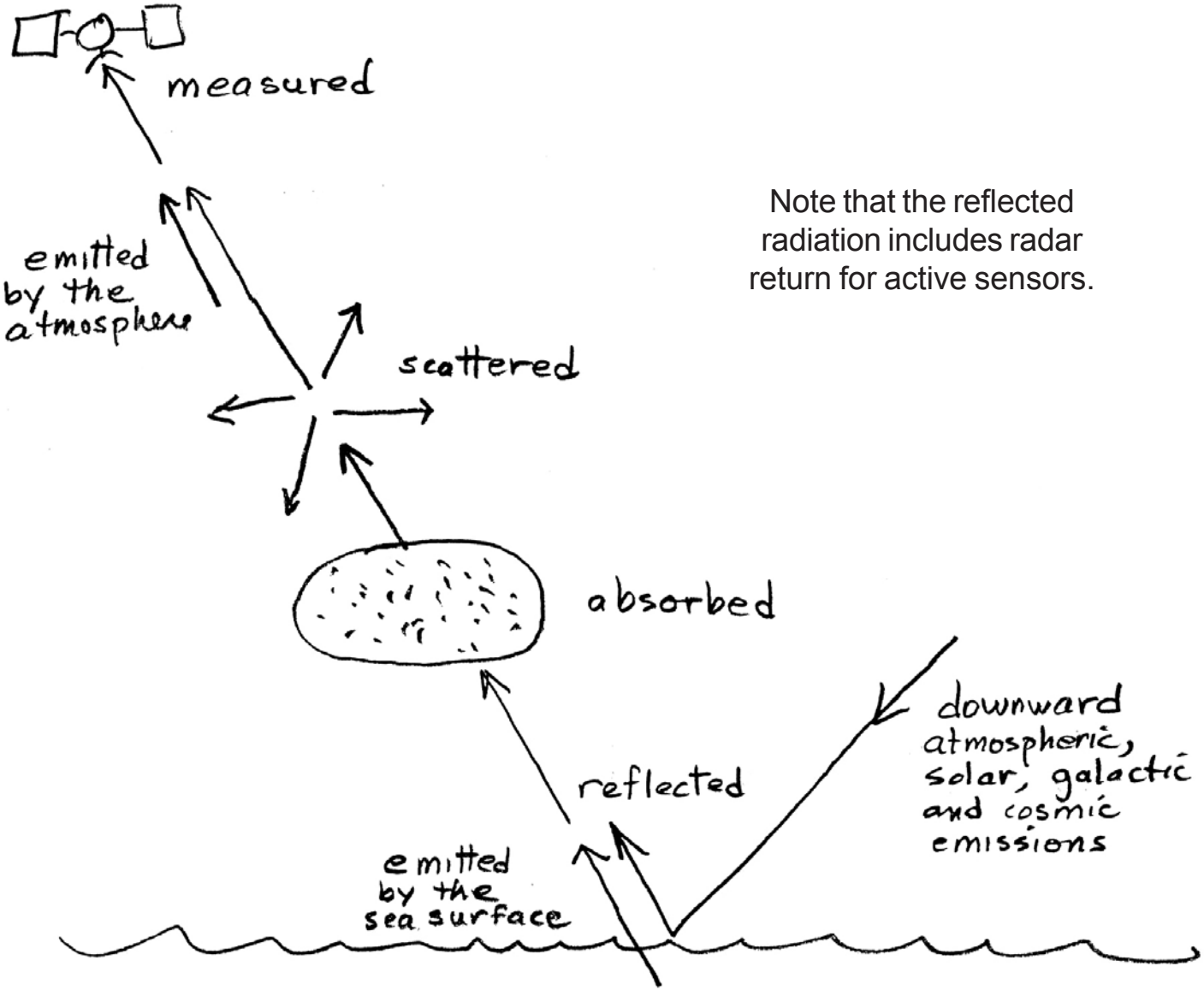


Note that the reflected radiation includes radar return for active sensors.

# Summary of Atmospheric Radiative Transfer

The preceding discussion summarized the radiative transfer of EMR as it propagates through the atmosphere to the radiometer onboard the satellite.

The water-leaving spectral radiance $L^f_w$ that is of interest for remote sensing of the physical characteristics of the sea surface (SST, wind speed and direction, sea surface height, color and salinity) is contaminated by numerous effects:

- *Visible measurements are contaminated by scattered spectral radiance $L^f_p$ from atmospheric gas molecules and aerosols, and are obscured completely by clouds.*
- *Infrared measurements are contaminated by the spectral radiance $L^f_e$ from thermal emission by atmospheric gases, scattered radiance $L^f_p$ from aerosols (at the short infrared wavelengths), and are obscured completely by clouds.*
- *Microwave measurements are contaminated by reflected spectral radiance $L^f_r$ from a variety of sources and by the radiance $L^f_e$ from thermal emission by atmospheric gases*

*In all three types of measurements, the water-leaving spectral radiance $L^f_w$ is attenuated by the atmosphere (i.e., the atmospheric transmittance is less than 1).*

$$L^f_m = t^f \left( L^f_w + L^f_r \right) + L^f_e + L^f_p$$

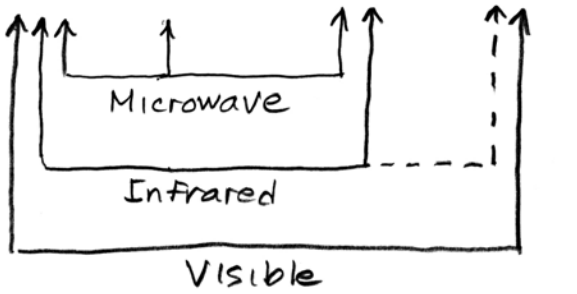

# Diffraction for Microwave versus Visible and Infrared Radiometers

Consider a lens with diameter D = 1 cm. Diffraction for visible and infrared optical radiometers with this aperture diameter scales as:

$$\text{Diffraction} \sim \frac{\lambda}{D}$$

$$\text{Visible } (\lambda \approx 0.3 \text{ to } 0.7\,\mu m): \quad \frac{\lambda}{D} \sim 10^{-5} \text{ to } 10^{-4}$$

$$\text{Infrared } (\lambda \approx 1 \text{ to } 100\,\mu m): \quad \frac{\lambda}{D} \sim 10^{-4} \text{ to } 10^{-2}$$

The wavelengths of microwave EMR are about 1-10 cm for the 1-50 GHz frequencies used for microwave remote sensing of the ocean. The lens diameter necessary to achieve the same degree of diffraction as with the optical lenses used in visible and infrared remote sensing is:

For a microwave wavelength of $\lambda = 1$ cm

$$\frac{\lambda}{D} = 10^{-4} \Rightarrow D \approx 100 \text{ m}$$

This is obviously impractical. Even a lens size of 1 m is impractical. The “lens” for the Hubble Space Telescope, for example, consisted of a 3-m mirror rather than a lens because it was lighter, cheaper and easier to build (even though it was built incorrectly).

*Microwave radiometers measure the spectral radiance with antennas rather than lenses or mirrors.*

# Microwave Antennas

Antennas are still limited by diffraction but, for the typical microwave antenna size of ~1 m, antennas are much lighter, less expensive, and easier to build than lenses.

Antennas are conducting materials that convert an oscillating incident electric field to an AC current, which is then band-pass filtered to measure the desired EMR within the desired frequency band.

The angular dependence of the field of view measured by an antenna is called the antenna gain pattern. The detailed shape of the antenna gain pattern depends on how the antenna is illuminated. The desired illumination is achieved by careful design of the reflector that focuses the incoming EMR on the antenna conductor, as shown schematically to the right.


*Most of the focused radiance falls near the center of the antenna conductor, with tapering to the sides of the conductor.*

The effects of two idealized illumination patterns on the antenna gain pattern are shown schematically in the figure to the right from a 1-dimensional cross section of the antenna.

- *For uniform illumination, the antenna gain pattern consists of a narrow main lobe and several significant sidelobes.*
- *The sidelobes can be reduced by tapering the illumination, but at the expense of broadening the main lobe.*

*The antenna sidelobes are the diffraction pattern for an antenna.*

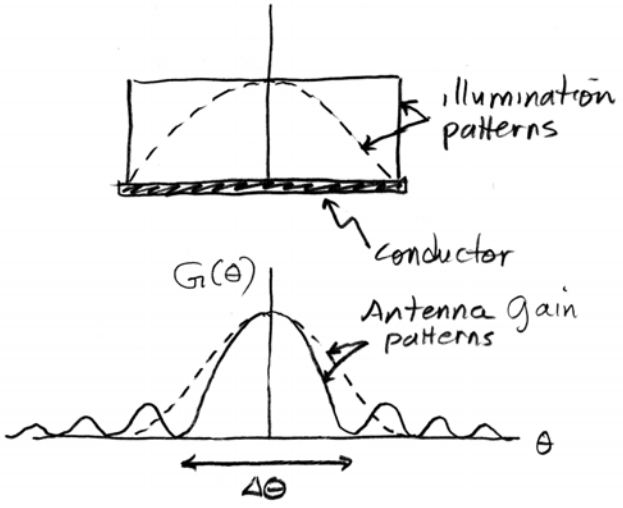

# Footprint Size

Regardless of the precise illumination of the antenna conductor, the beamwidth is approximately $\Delta\theta \approx \frac{\lambda}{D} = \frac{c_o}{Df}$

The beamwidth is thus inversely related to the antenna diameter D. The antenna beamwidth defines the instantaneous field of view (IFOV) of the antenna, which in turn defines the footprint size on the sea surface. Since the beamwidth is small, the footprint diameter for measurements from an altitude of H is $d \approx H\Delta\theta \approx \frac{Hc_o}{Df}$

=> *High-resolution measurements (small footprint size) require a large antenna diameter.*

Note that the footprint size for a given antenna diameter D increases linearly with decreasing microwave frequency.

Likewise, reducing the footprint size for a given microwave frequency can be achieved only by increasing the antenna diameter D.

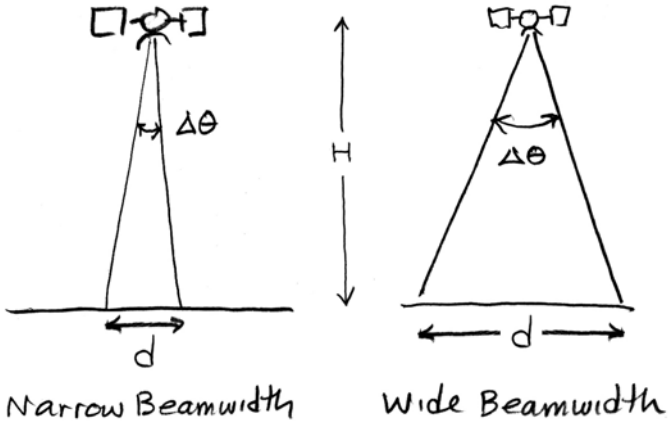

# Interpretation of Microwave Brightness Temperature

After correcting the measured spectral radiance $L_m^f$ for:

- *atmospheric attenuation of the water-leaving radiance* $T_w^f$
- *the reflected spectral radiance* $L_r^f$

and applying the antenna pattern correction to reduce contamination from the antenna sidelobes, the brightness temperature $T_b^f$ computed from $L_m^f$ is interpreted as the average "scene temperature" within the field of view of the main lobe of the antenna gain pattern,

$$T_b^f = e\,T$$

where T is the physical temperature of the material in the field of view (the sea surface or the intervening atmosphere, depending on the frequency as discussed later), and e is the emissivity of the material.

It is evident that $T_b^f$ can change either from changes in T or from changes in e. Recall that

$$e = e(pol, \theta, \epsilon_r, \lambda)$$

The electrical properties of the sea surface (i.e., the dielectric constant $\epsilon_r$), and therefore the emissivity e, depend on the temperature, salinity and roughness of the sea surface as shown below.

# Summary of Brightness Temperature Sensitivities to Salinity, SST, Wind Speed, Water Vapor and Cloud Liquid Water

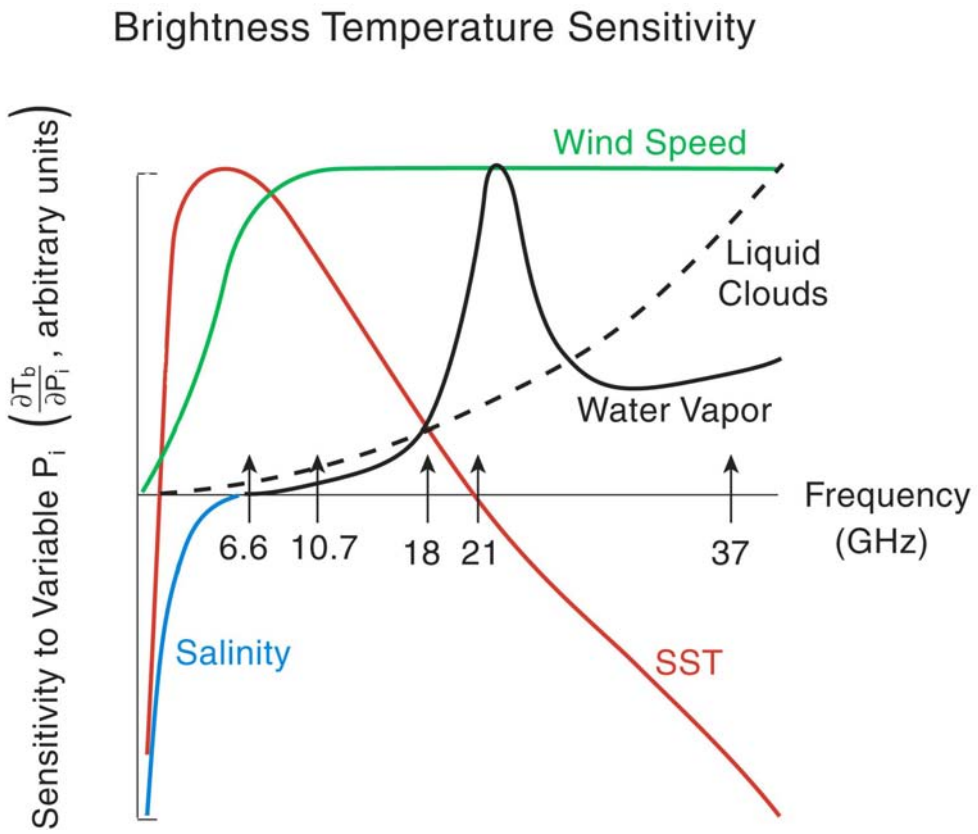


The sensitivities of brightness temperature $T_b$ to changes in the various physical effects on emissivity are summarized in the figure to the left.

Based on these results, an "optimal" combination of microwave frequencies for estimation of these 5 variables is:

- *~1.4 GHz for salinity*
- *~7 GHz for SST*
- *~10.7 GHz for wind speed*
- *~19 and 22 GHz for water vapor (the difference between the $T_b$ at these two frequencies provides a more accurate estimate of water vapor than does $T_b$ at just one freq.)*
- *~37 GHz for cloud liquid water (which is well below the 50-70 GHz $O_2$ absorption band)*

# Caveats in Microwave Estimation of SST

The primary limitations of microwave estimates of SST are:

- *the large footprint size of ~50 km, compared with ~1 km for infrared estimates of SST.*
- *the inability to measure SST closer than about 1.5 footprints from land because of antenna sidelobe contamination.*

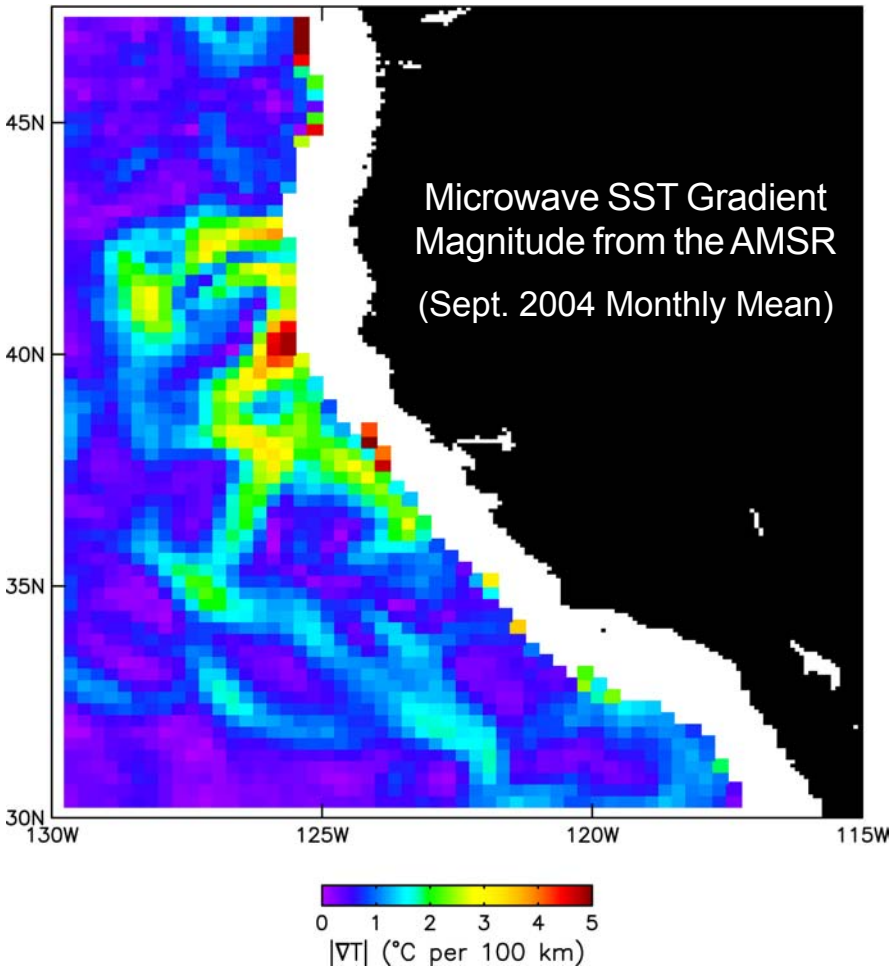


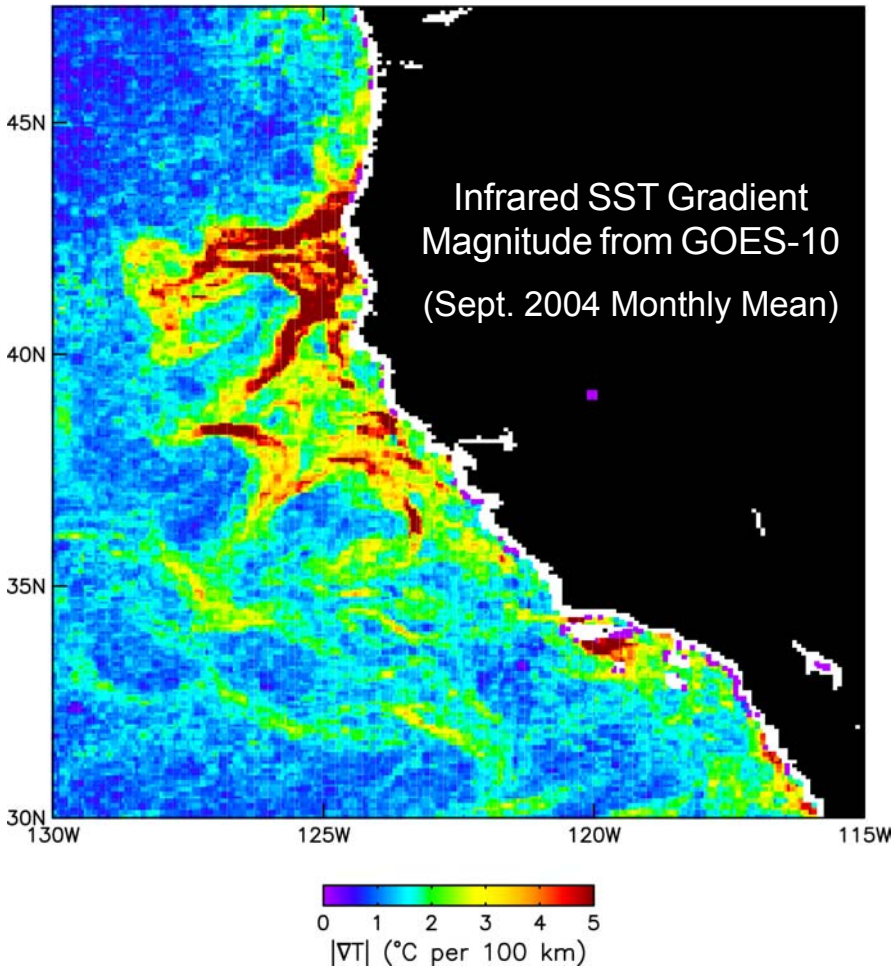

# Microwave SST Missions

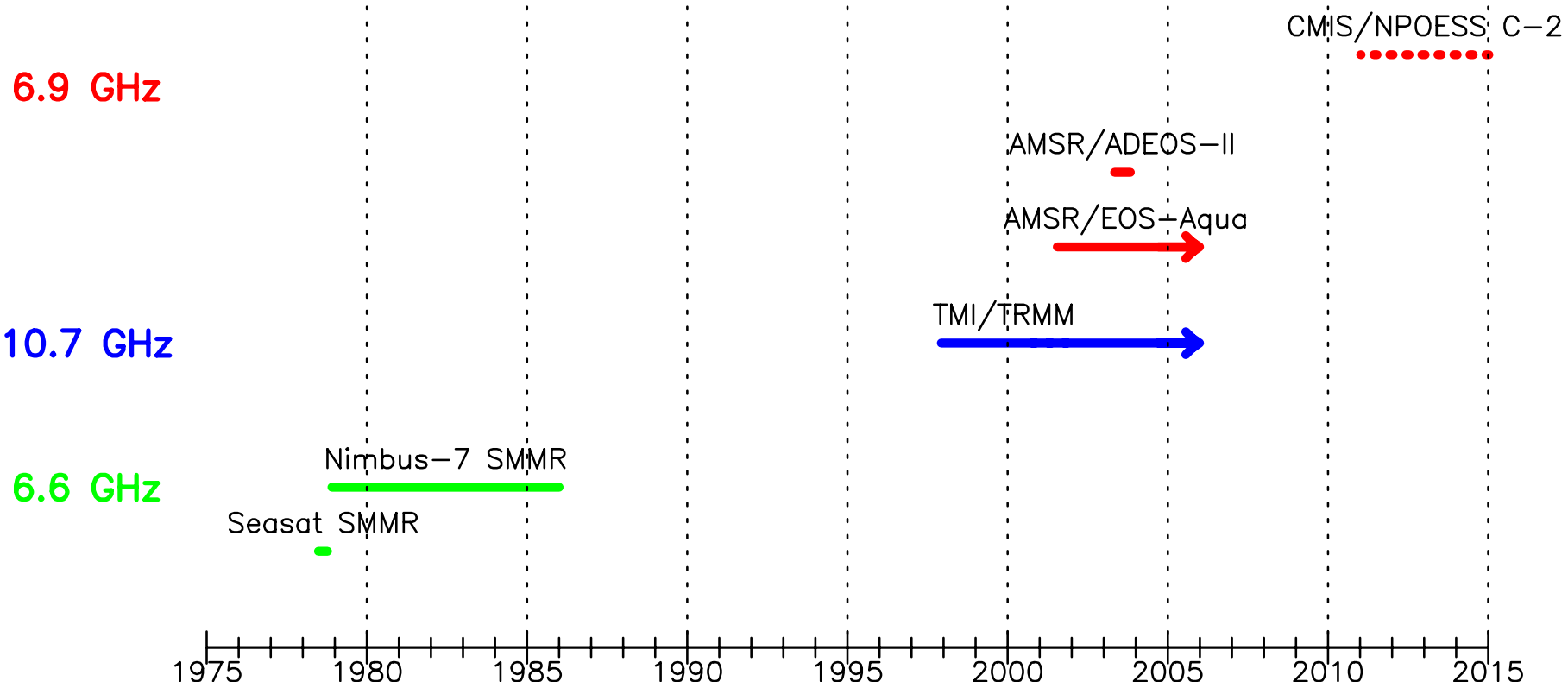

# Examples of Microwave Measurements of Sea-Surface Temperature

Tropical Instability Waves in the Eastern Tropical Pacific

The SST front along the Agulhas Return Current

The Gulf Stream

The Kuroshio Extension

*(more examples later in combination with scatterometer measurements of surface winds)*

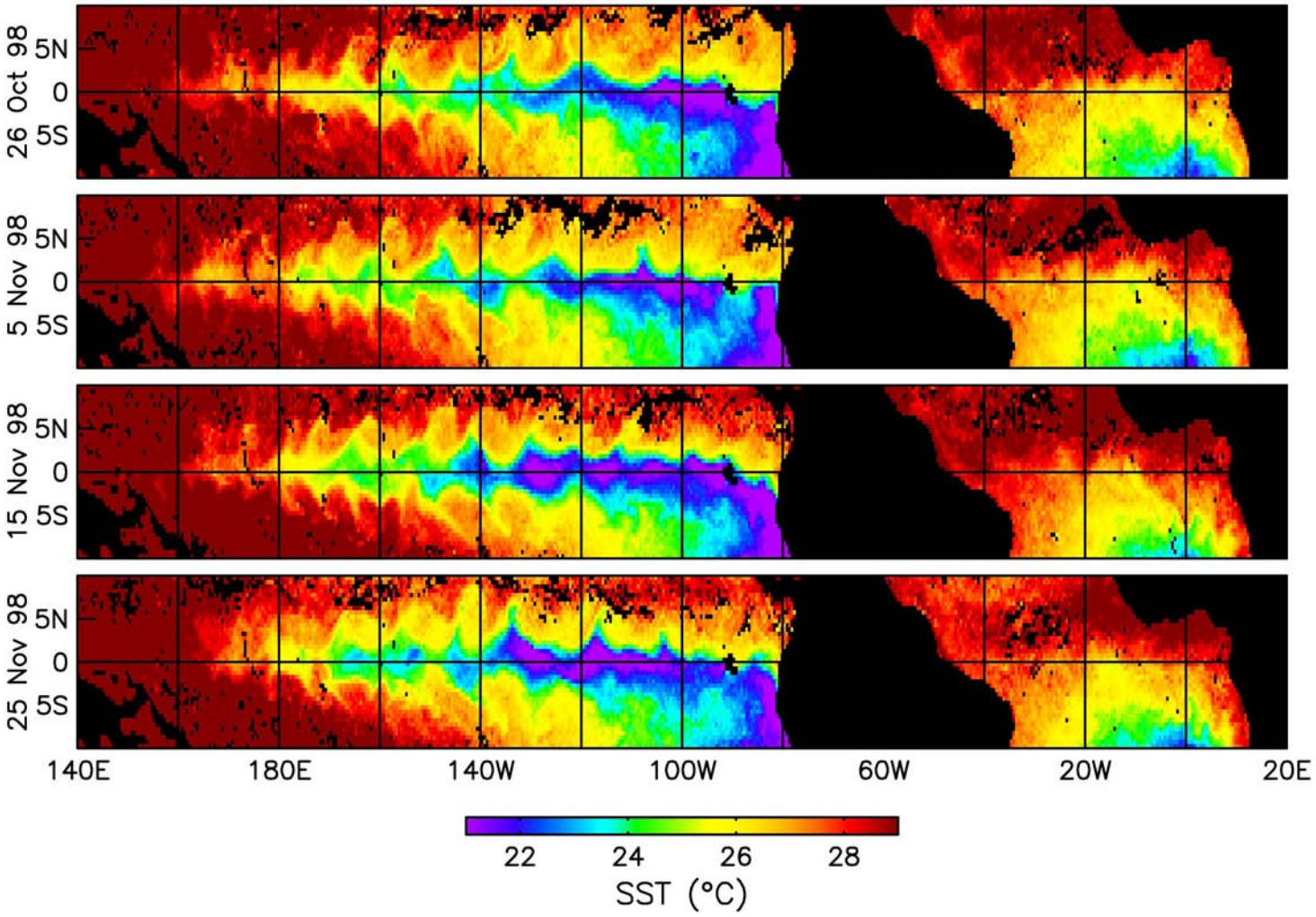
26 Oct 98
5N
0
5S
5 Nov 98
5N
0
5S
15 Nov 98
5N
0
5S
25 Nov 98
5N
0
5S
140E
180E
140W
100W
60W
20W
20E
22
24
26
28
SST (°C)

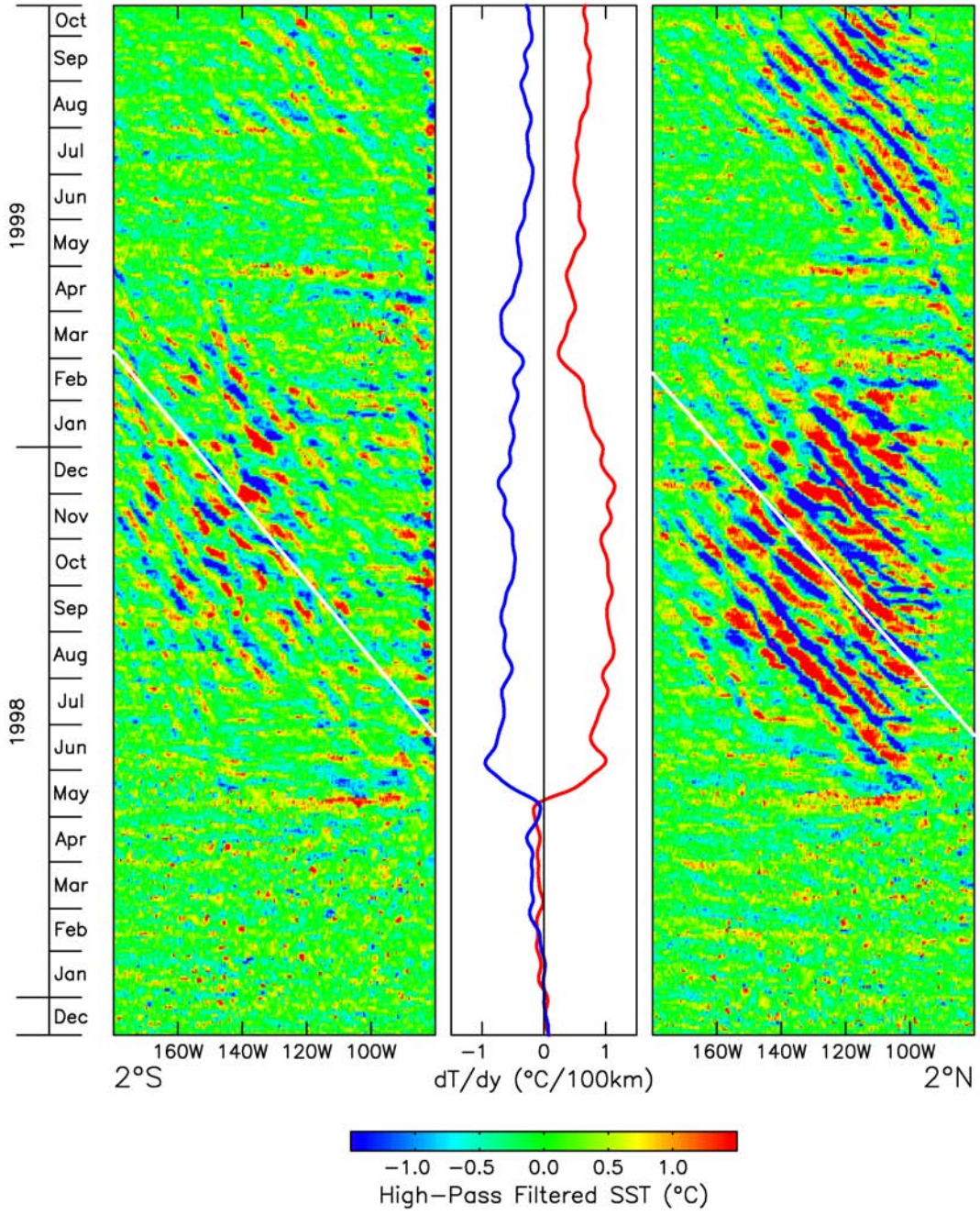
1999
1998
Oct
Sep
Aug
Jul
Jun
May
Apr
Mar
Feb
Jan
Dec
Nov
160W 140W 120W 100W
2°S
−1 0 1
dT/dy (°C/100km)
160W 140W 120W 100W
2°N
−1.0 −0.5 0.0 0.5 1.0
High−Pass Filtered SST (°C)

# Percent Coverage of Microwave versus Infrared Measurements of SST

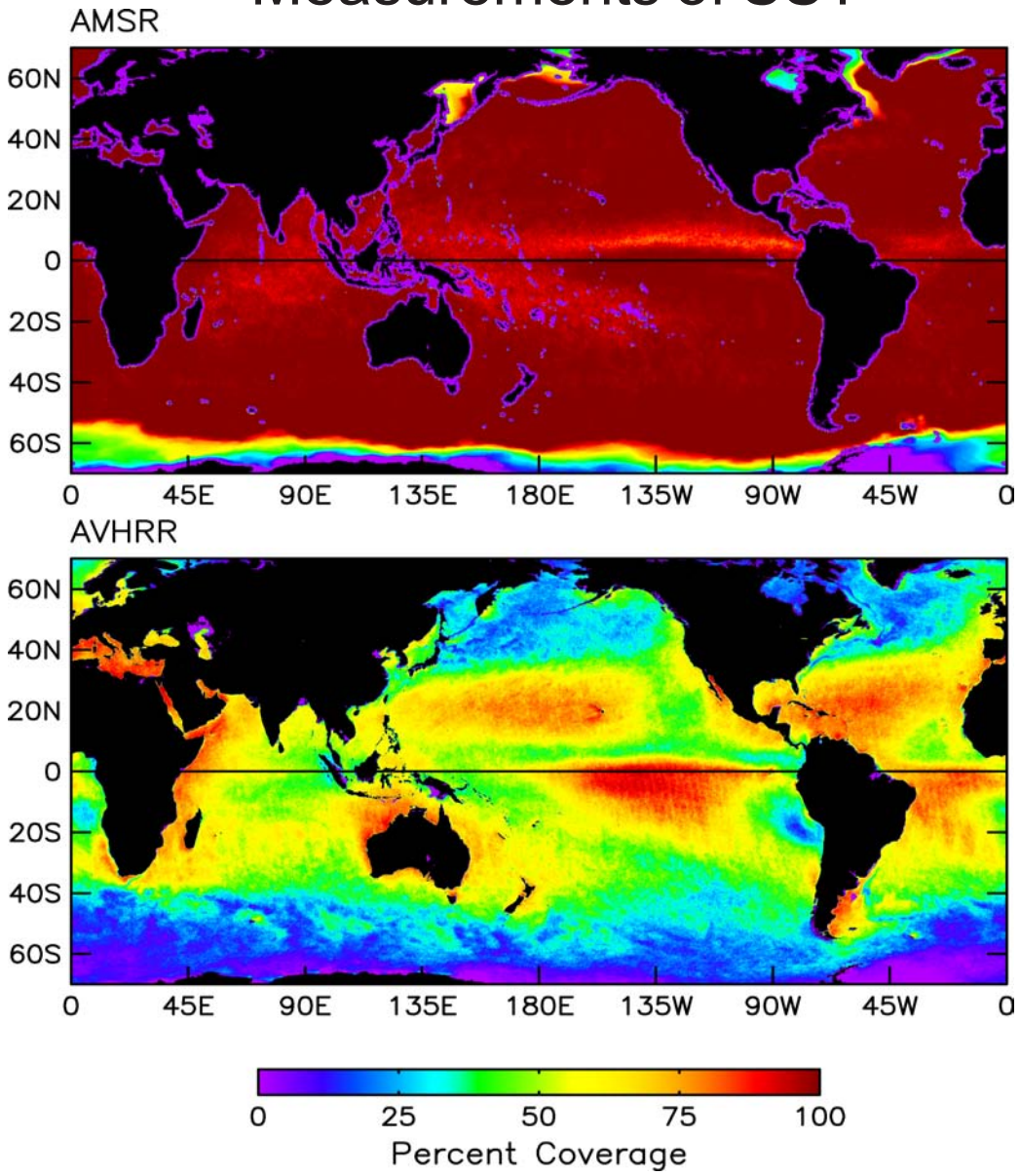

# Agulhas Return Current (South Indian Ocean)

5 July 2002

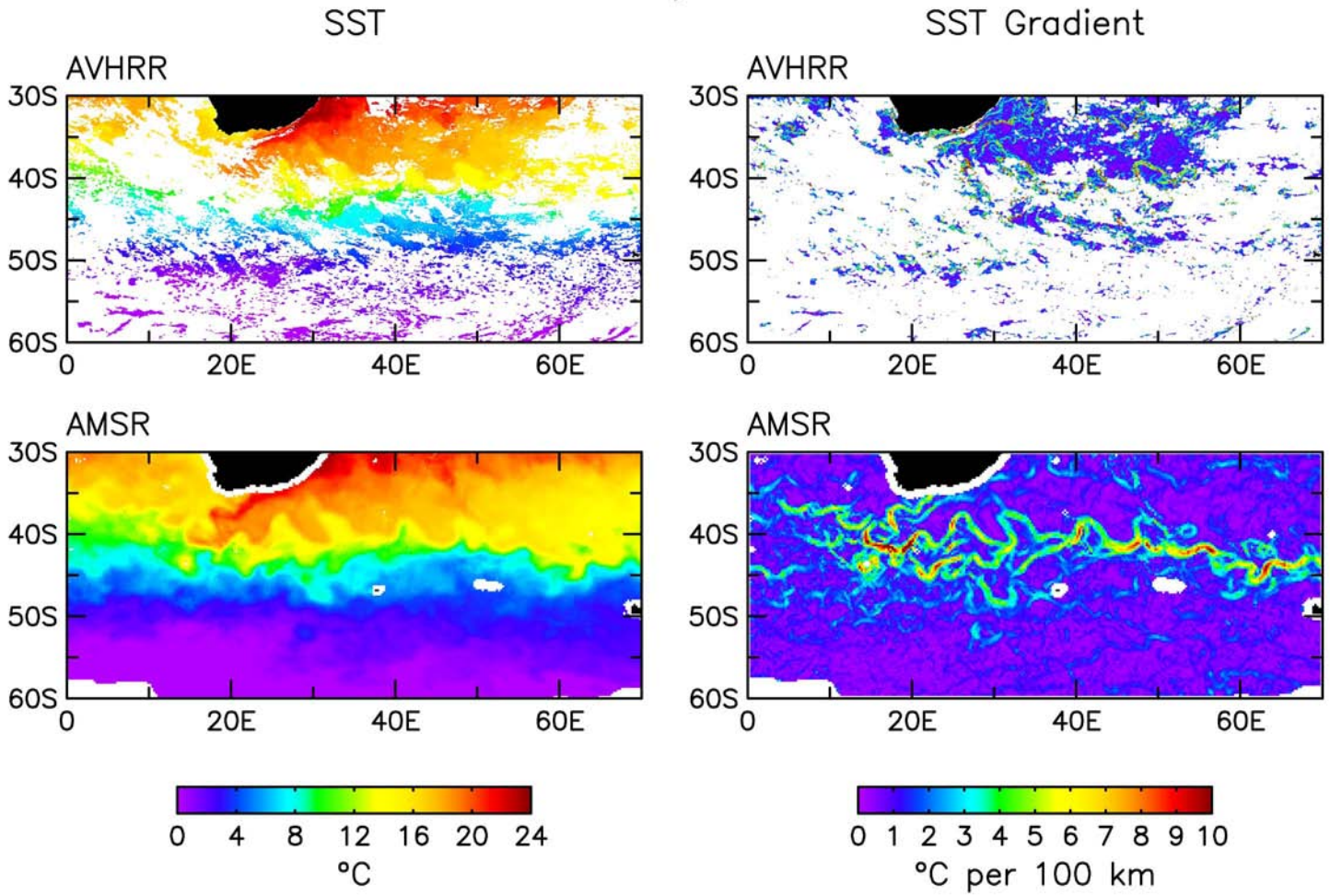

# Gulf Stream (North Atlantic Ocean)

1 May 2003

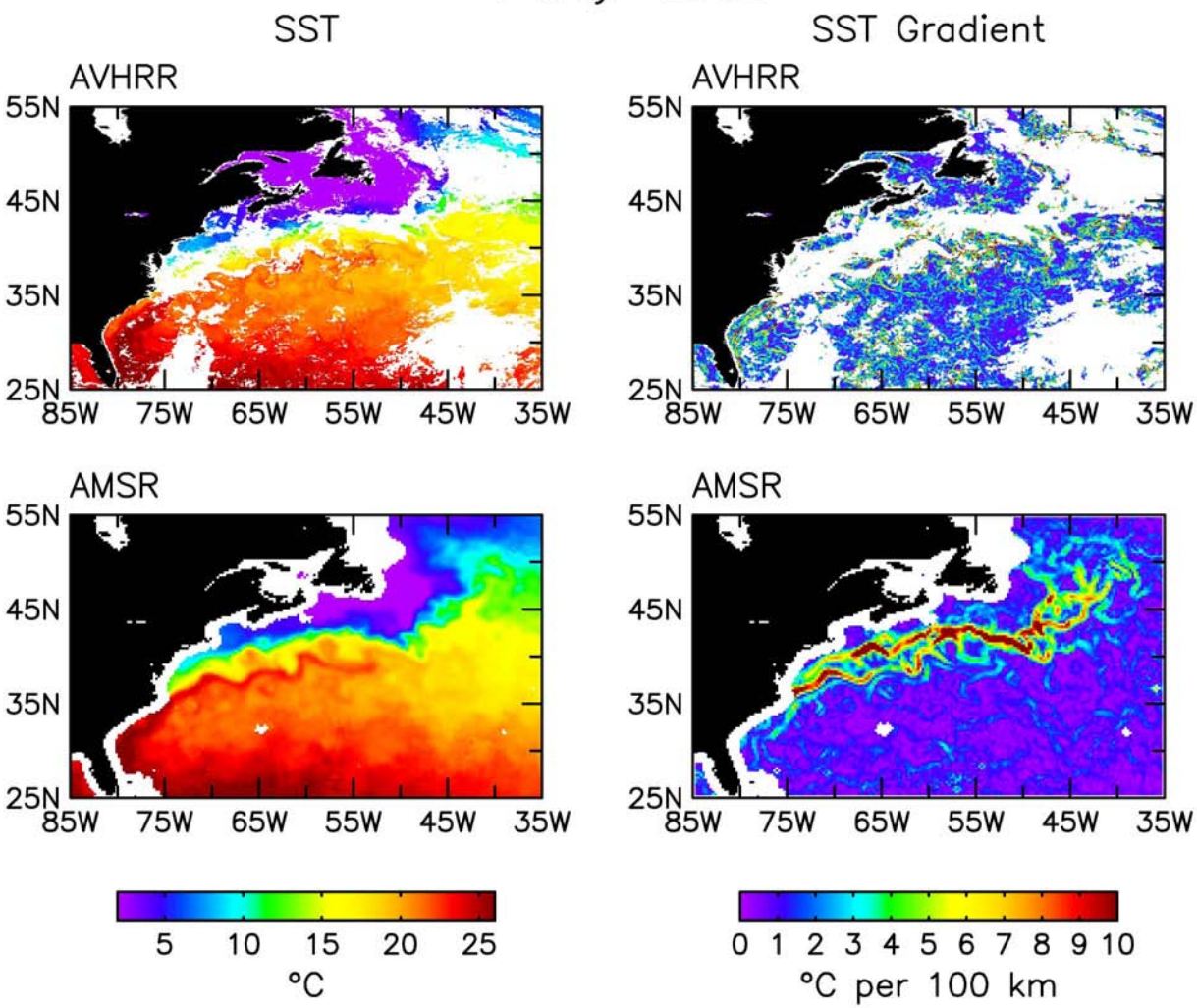

# Kuroshio Extension (North Pacific Ocean)

10 June 2003

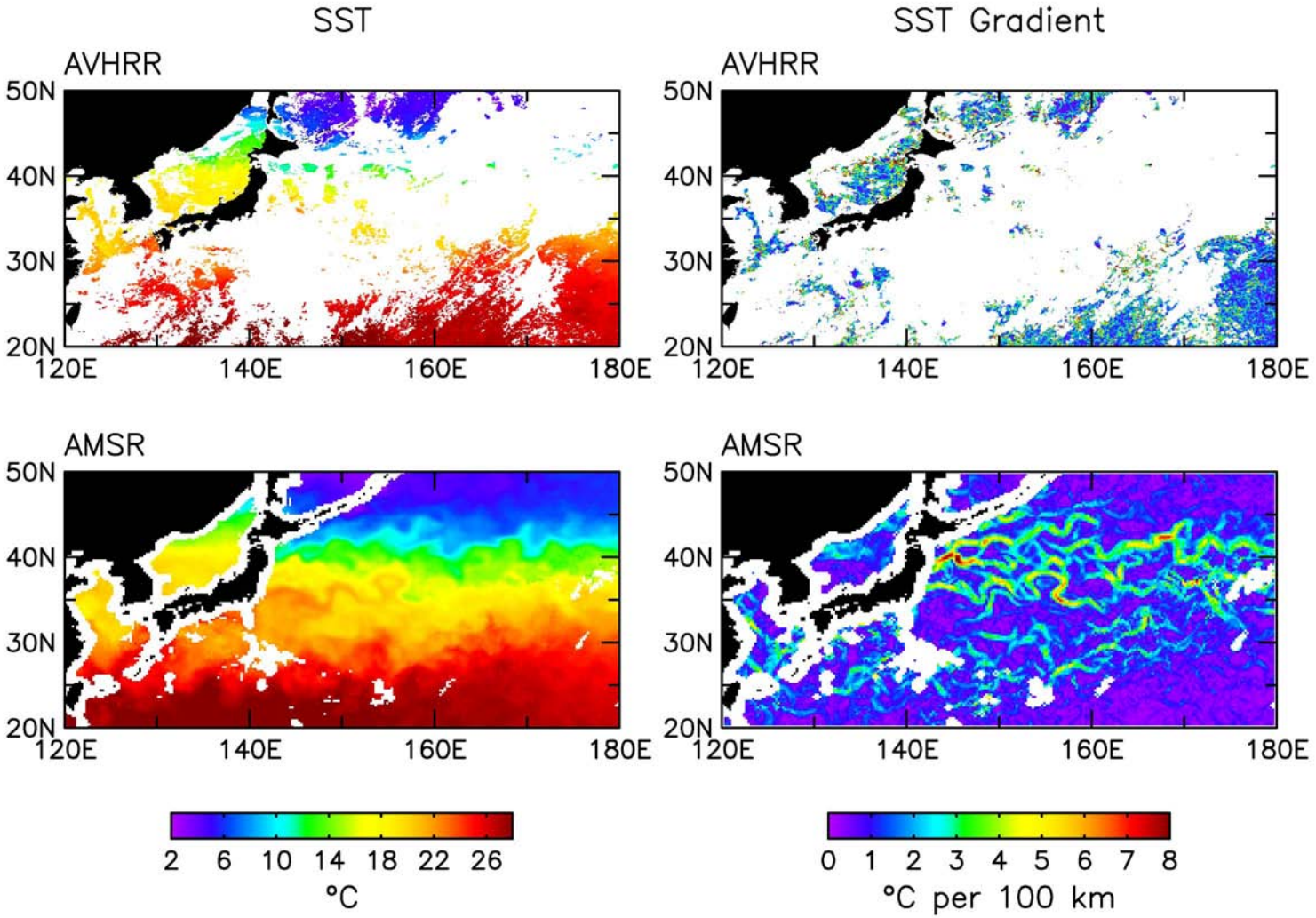

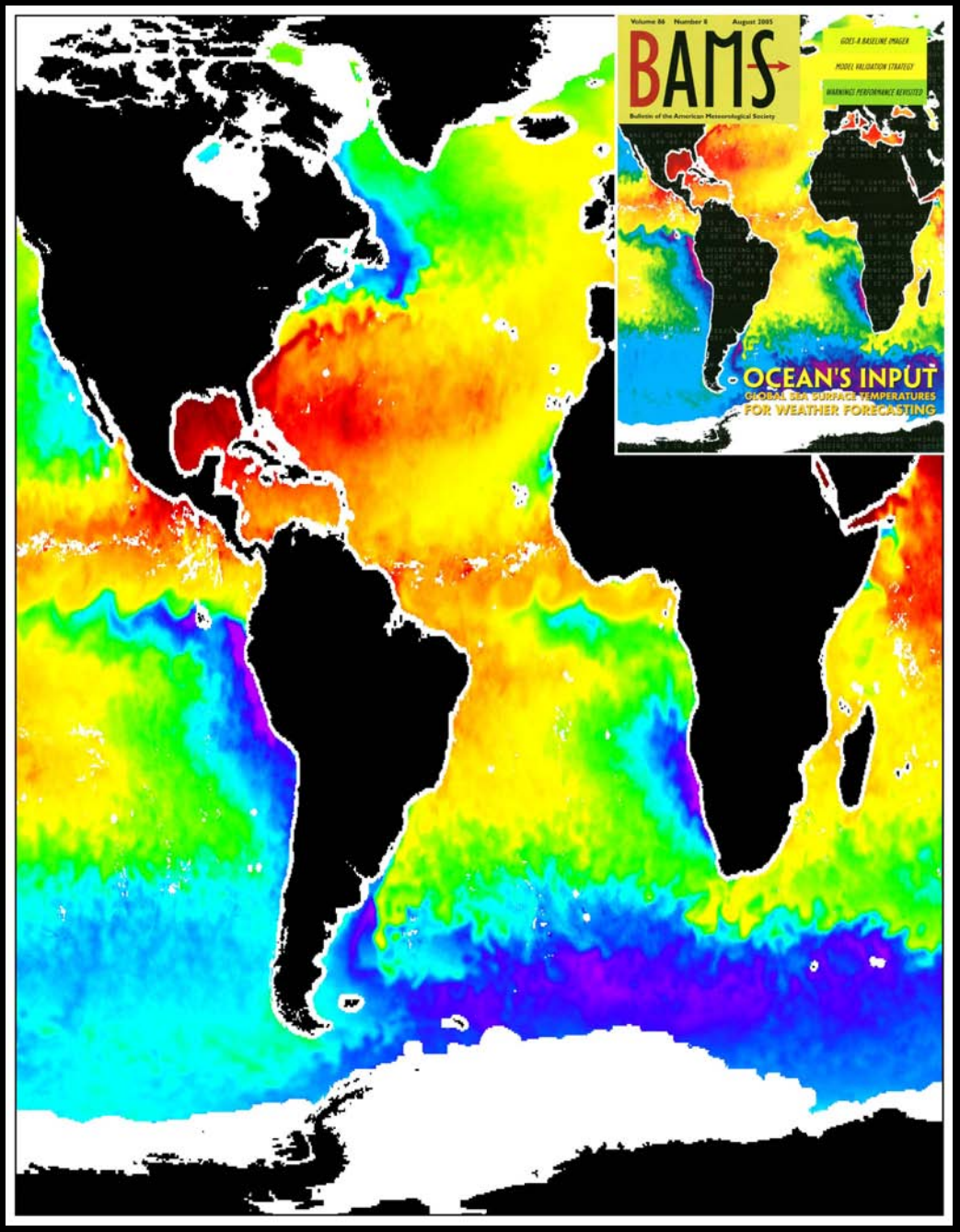
Volume 86 Number 8 August 2005
BAMS
Bulletin of the American Meteorological Society
GOES-R BASELINE IMAGER
MODEL VALIDATION STRATEGY
WARNINGS PERFORMANCE REVISITED
OCEAN'S INPUT
GLOBAL SEA SURFACE TEMPERATURES
FOR WEATHER FORECASTING

# SST Animation

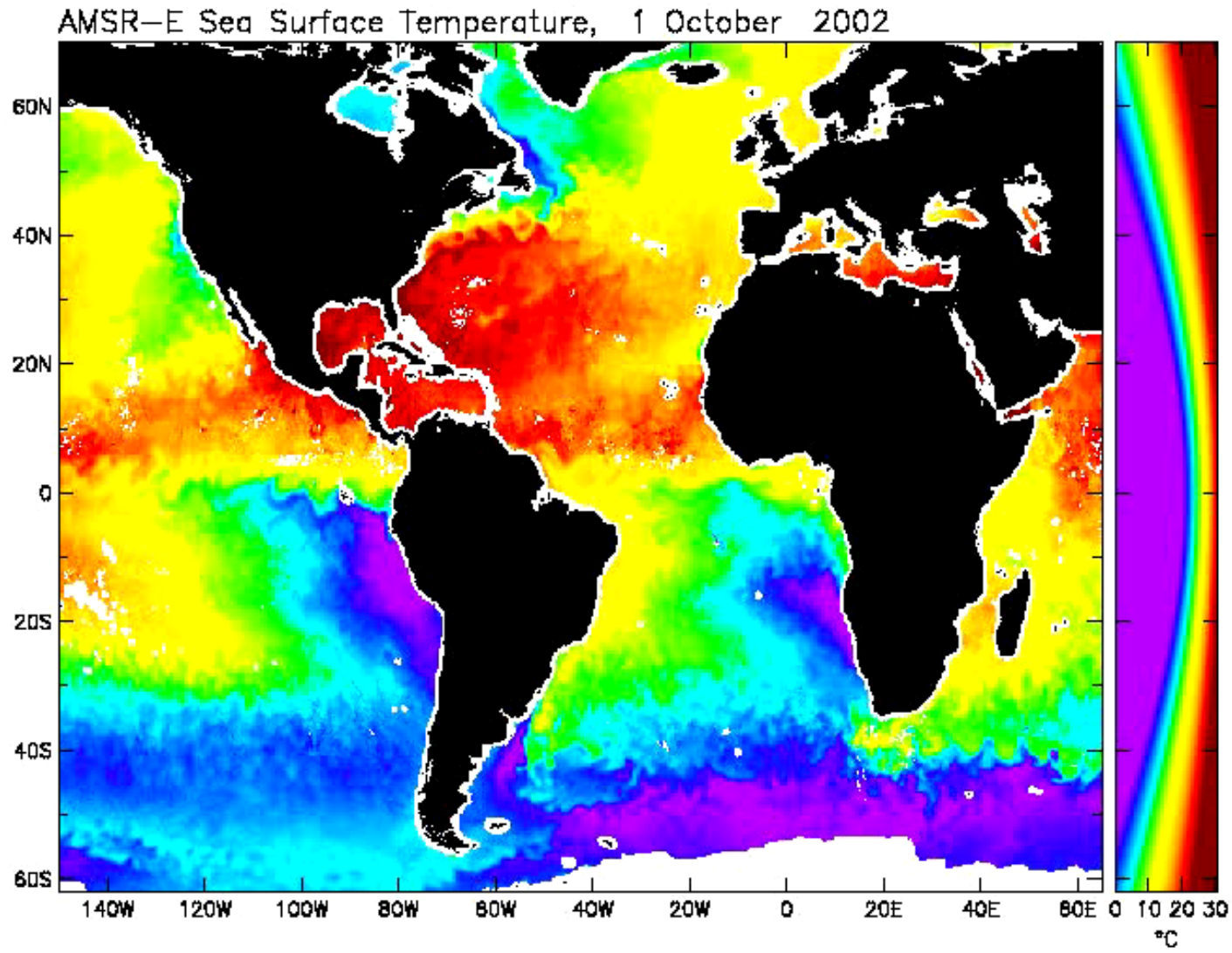

# Radar Altimetry


TOPEX/POSEIDON Launch
August 10, 1992
Kourou, French Guiana

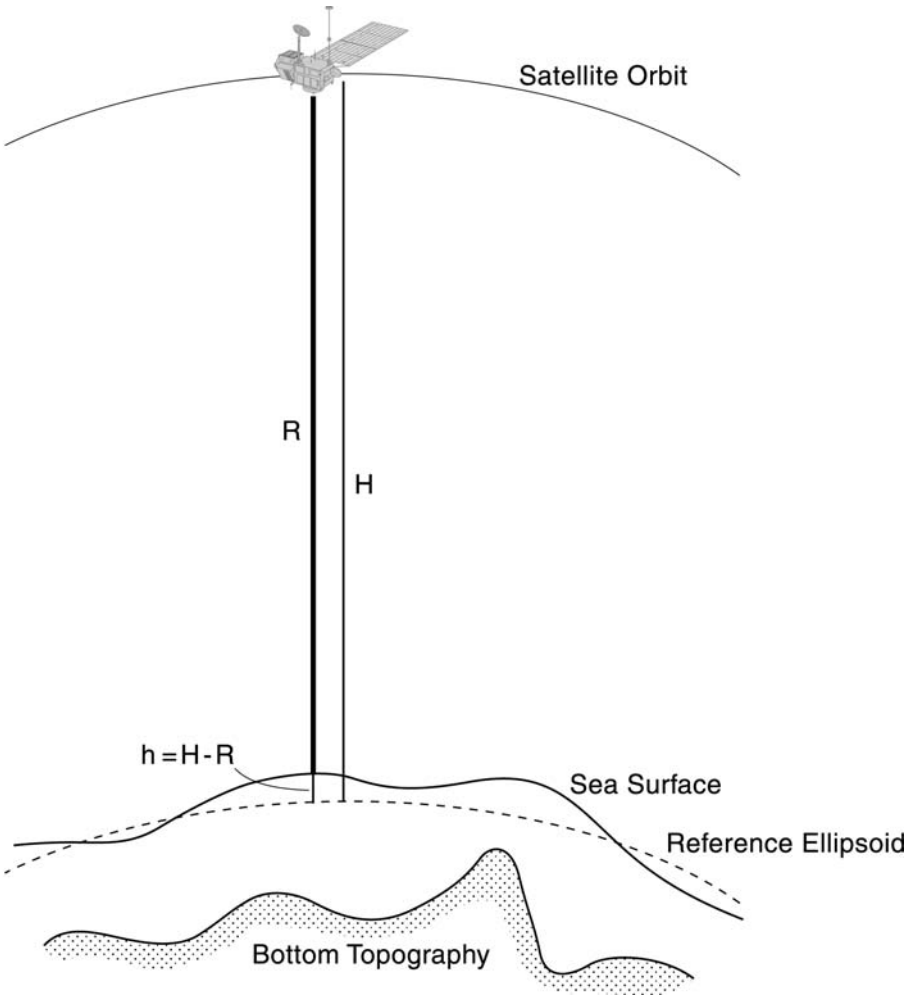
Satellite Orbit
R
H
h = H - R
Sea Surface
Reference Ellipsoid
Bottom Topography

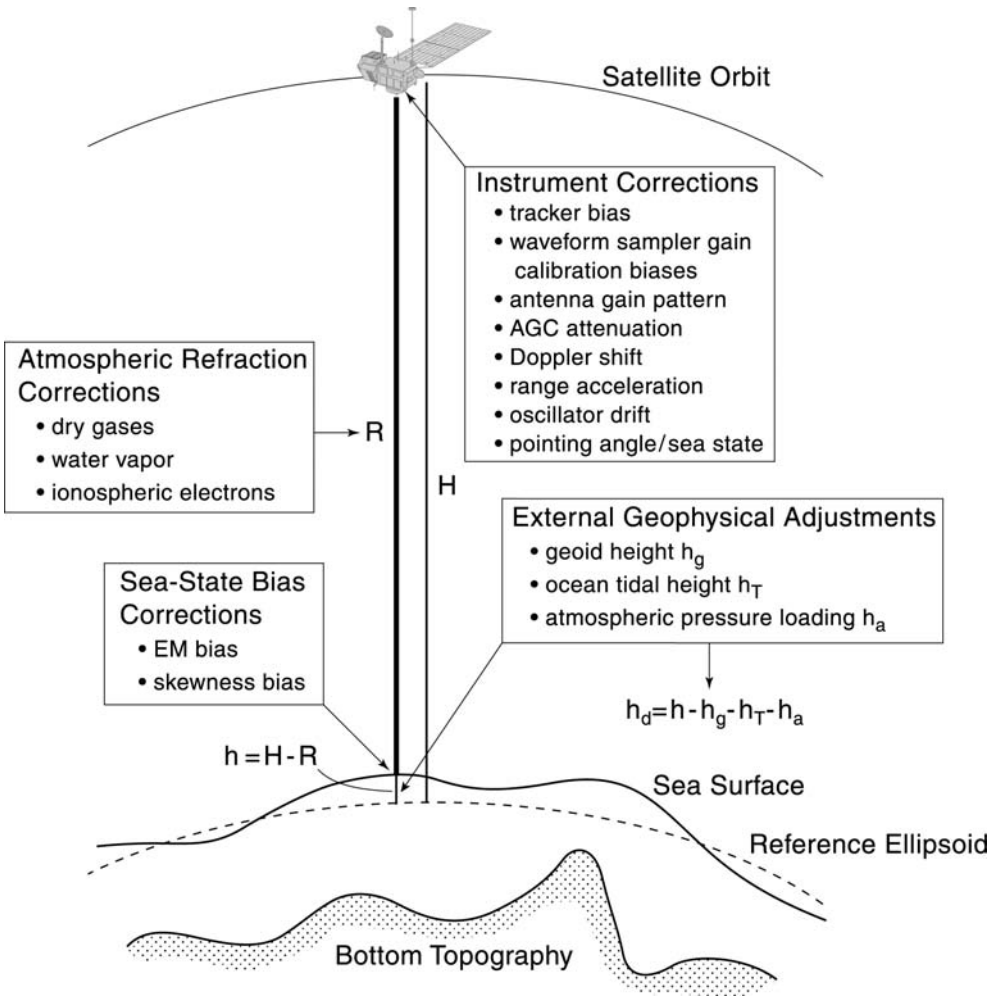


$$h = H - R$$
$$= H - \left( \hat{R} - \sum_j \Delta R_j \right)$$

$R =$ $\hat{R} - \sum_j \Delta R_j$ is the range between the satellite and the sea surface.

$\hat{R} =$ $c_0 t/2$ is the range computed from the altimeter measurements of the 2-way travel time $t$ of radar pulses neglecting refraction, i.e., based on the free-space speed of light $c_0$.

$\Delta R_j =$ Corrections for the various components of atmospheric refraction (dry gases, water vapor, cloud liquid water and ionospheric electrons) and for biases between the mean electromagnetic scattering surface and mean sea level at the air-sea interface.

$H =$ The height of the satellite above a reference ellipsoid approximation of the Earth's surface, determined from ground-based tracking and GPS.

$h =$ The height of the sea surface relative to the reference ellipsoid.

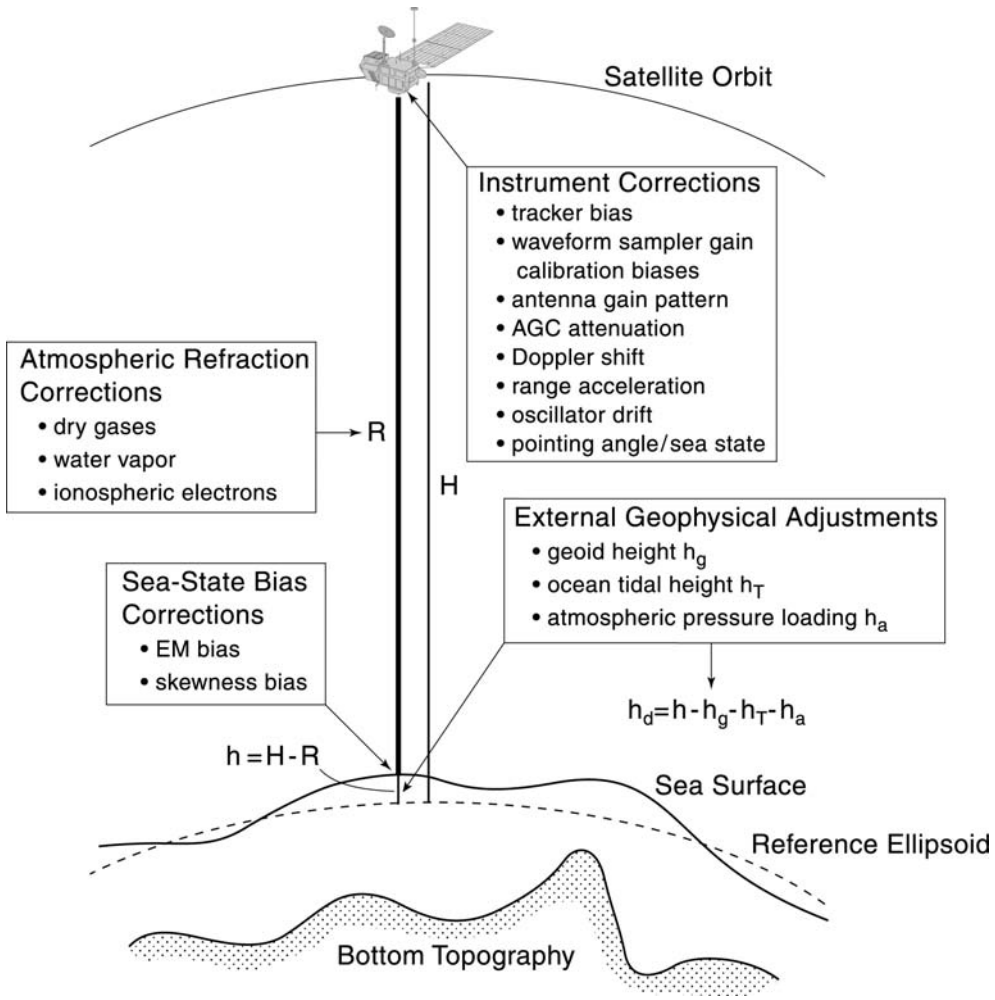


$$h = H - R$$
$$= H - \left( \hat{R} - \sum_j \Delta R_j \right)$$

$R =$ $\hat{R} - \sum_j \Delta R_j$ is the range between the satellite and the sea surface.

$\hat{R} =$ $c_0 t/2$ is the range computed from the altimeter measurements of the 2-way travel time $t$ of radar pulses neglecting refraction, i.e., based on the free-space speed of light $c_0$.

$\Delta R_j =$ Corrections for the various components of atmospheric refraction (dry gases, water vapor, cloud liquid water and ionospheric electrons) and for biases between the mean electromagnetic scattering surface and mean sea level at the air-sea interface.

$H =$ The height of the satellite above a reference ellipsoid approximation of the Earth's surface, determined from ground-based tracking and GPS.

$h =$ The height of the sea surface relative to the reference ellipsoid.

$$h_d = h - h_g - h_T - h_a$$
$$= H - \left( \hat{R} - \sum_j \Delta R_j \right) - h_g - h_T - h_a$$

$h_d =$ The dynamic sea surface height from the effects of geostrophic currents.

$h_g =$ Undulations of the equipotential about the ellipsoidal approximation of the Earth's surface (the marine geoid).

$h_T =$ Tidal variations of the sea surface height.

$h_a =$ The sea surface response to atmospheric pressure loading (the "inverted barometer effect").

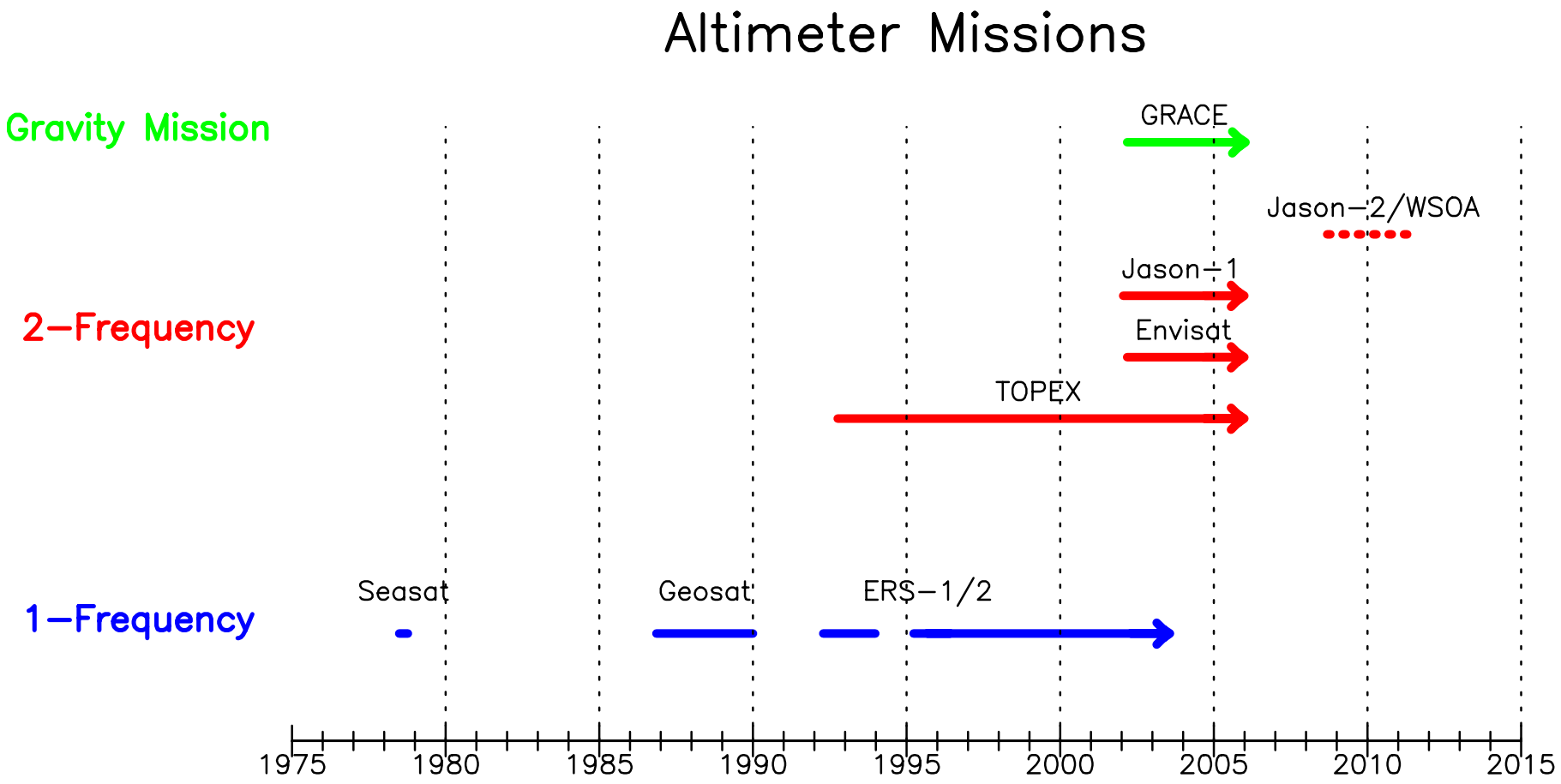
Altimeter Missions
Gravity Mission
2–Frequency
1–Frequency
GRACE
Jason–2/WSOA
Jason–1
Envisat
TOPEX
Seasat
Geosat
ERS–1/2
1975
1980
1985
1990
1995
2000
2005
2010
2015

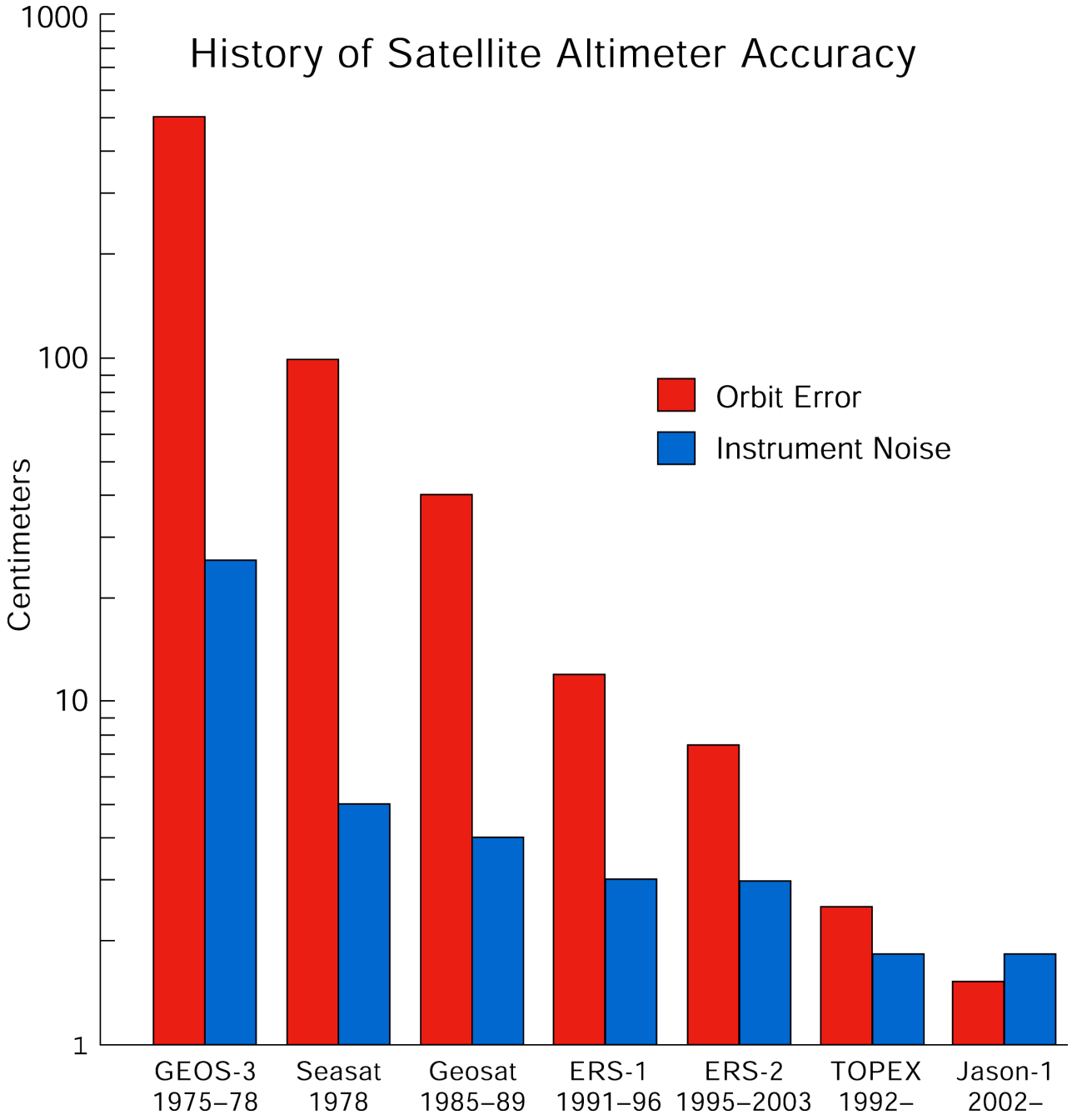
History of Satellite Altimeter Accuracy
Centimeters
1000
100
10
1
Orbit Error
Instrument Noise
GEOS-3
1975–78
Seasat
1978
Geosat
1985–89
ERS-1
1991–96
ERS-2
1995–2003
TOPEX
1992–
Jason-1
2002–

# Limitations of Altimeter Measurements of Sea Surface Height

*Uncertainties in the geoid height have limited oceanographic applications of altimeter data to studies of temporal variability.* Removal of the mean sea surface height eliminates the geoid, but unforunately also eliminates the mean sea surface height associated with mean geostrophic surface currents.

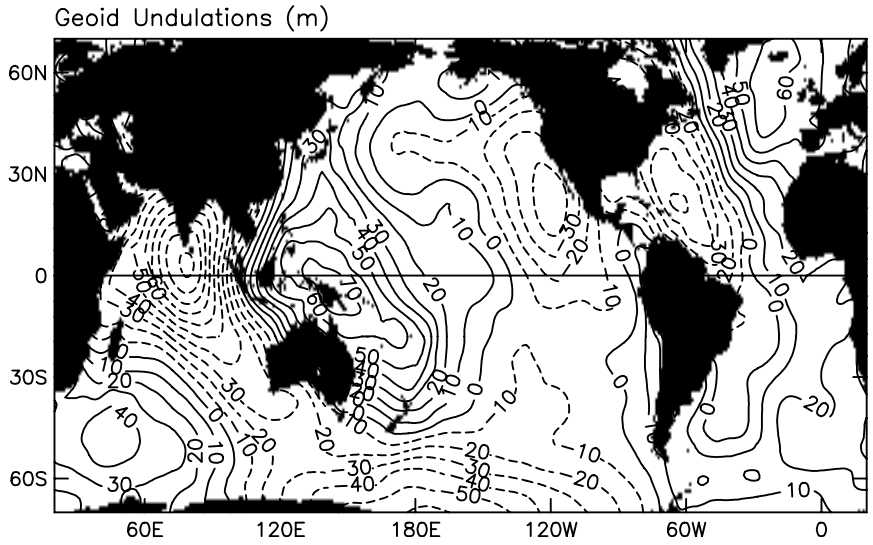


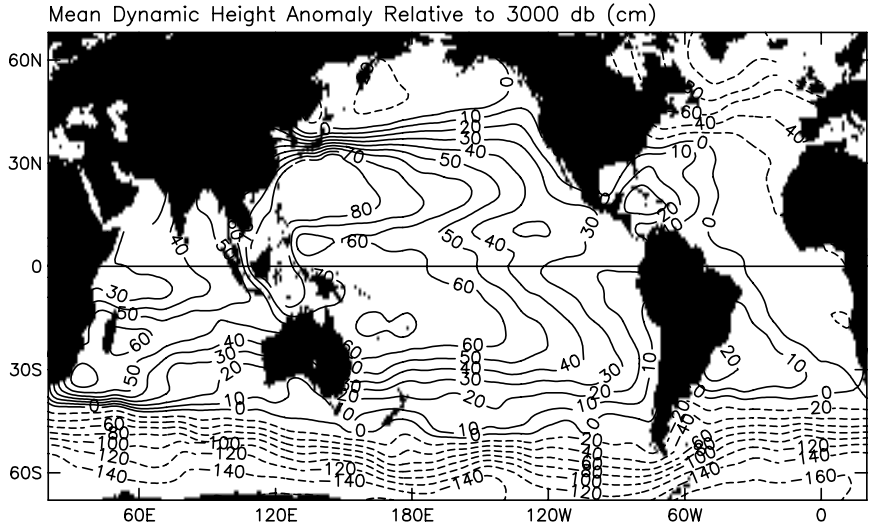


The dynamic range of the marine geoid is almost 200 m, which is about two orders of magnitude smaller than this.

Until recently, the accuracy of geoid height estimates has been limited to about 20 cm.

*The availability of gravity measurements from the Gravity Recovery and Climate Experiment (GRACE) mission is now providing geoid estimates with an estimated accuracy of better than 1 cm on length scales (half wavelength) longer than about 200 km.* Quantitative analyses of GRACE gravity estimates are just beginning to appear in the literature.

Gravity measurements from the future launch of the European Gravity Field and Steady-State Ocean Circulation Explorer (GOCE) with a planned launch in 2006 is expected to further improve the geoid measurement accuracy to about 1 cm on length scales down to 100 km.

Altimeter data can be analyzed retrospectively in the future using these accurate geoid estimates to investigate the mean ocean circulation and its interaction with eddy variability.

Meanwhile, *altimeter data have proven very useful for studies of the temporally varying ocean circulation.*

# Standard Deviation of Nonseasonal SSH

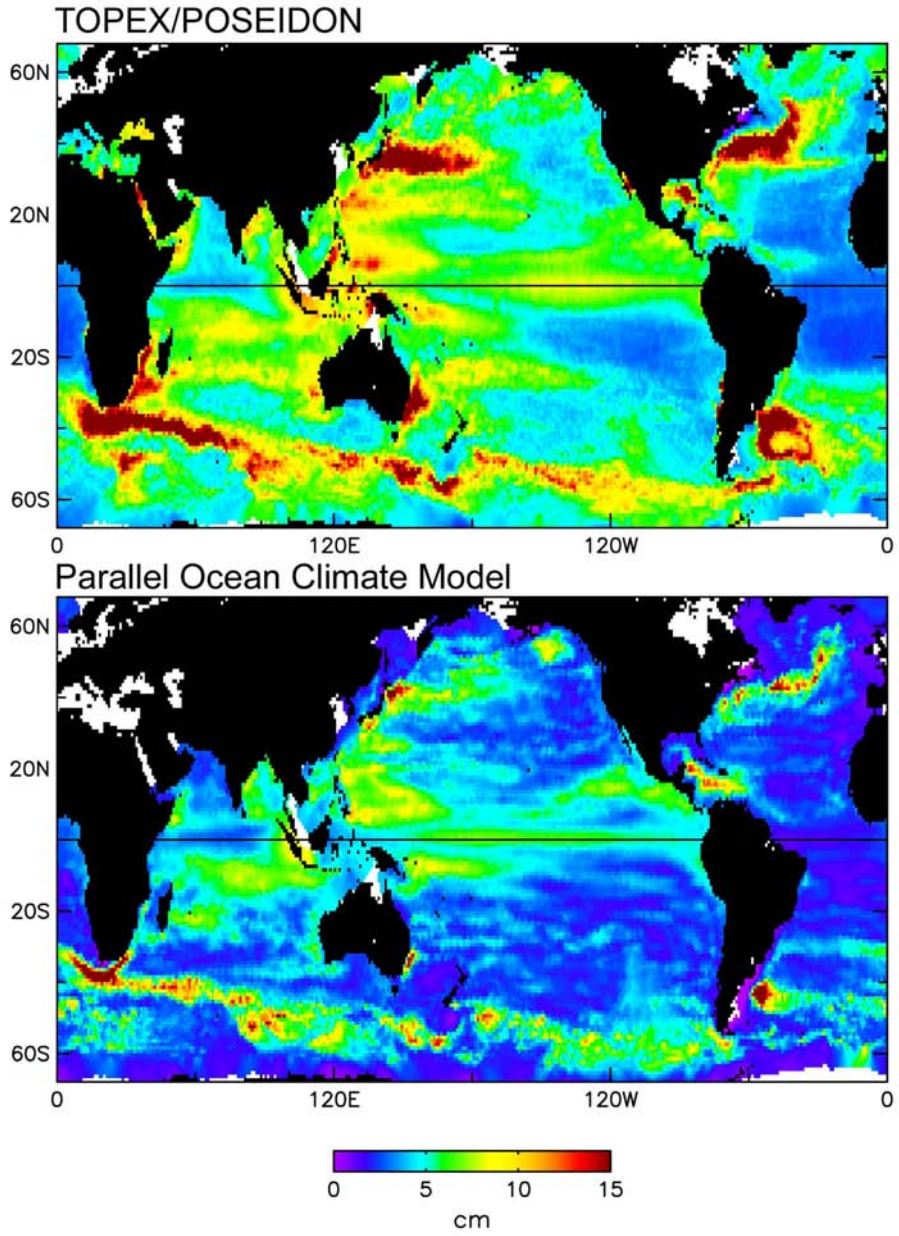

# Altimeter Estimates of Global Sea Level Rise

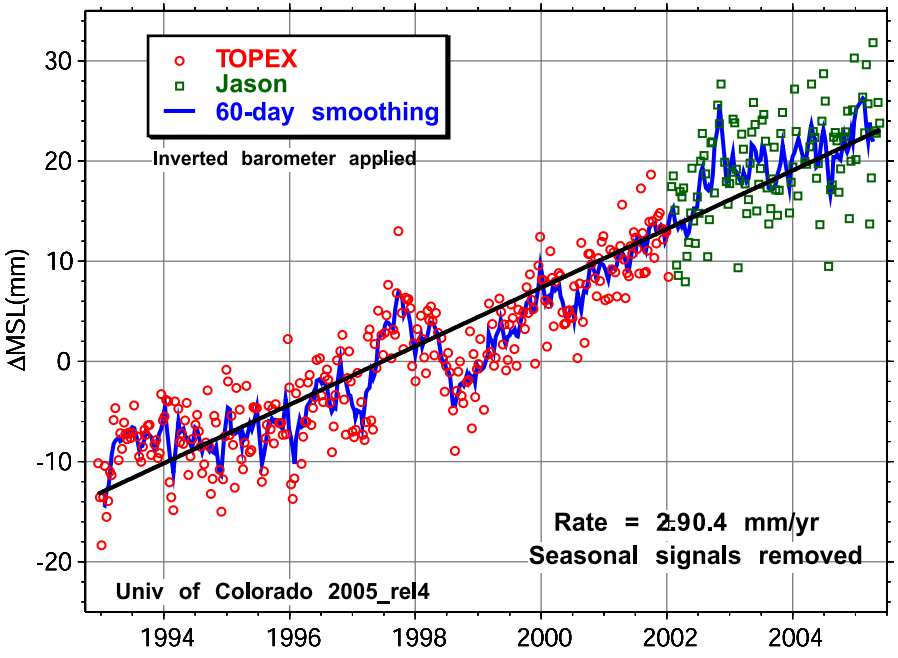


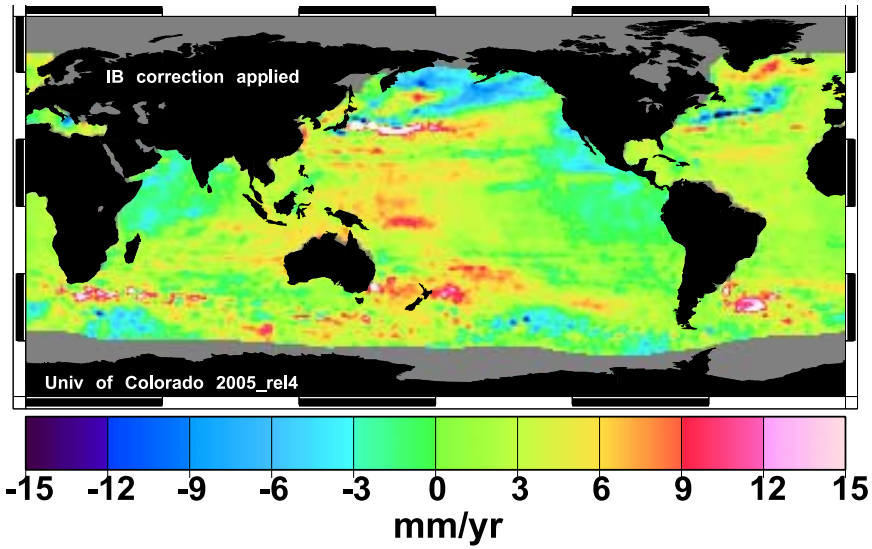


Leuliette, E. W, R. S. Nerem, and G. T. Mitchum, 2004: Calibration of TOPEX/Poseidon and Jason altimeter data to construct a continuous record of mean sea level change. *Marine Geodesy*, **27**(1-2), 79-94. (http://sealevel.colorado.edu)

# Observed SSH Variability in the North Pacific

October 1992 - August 2002

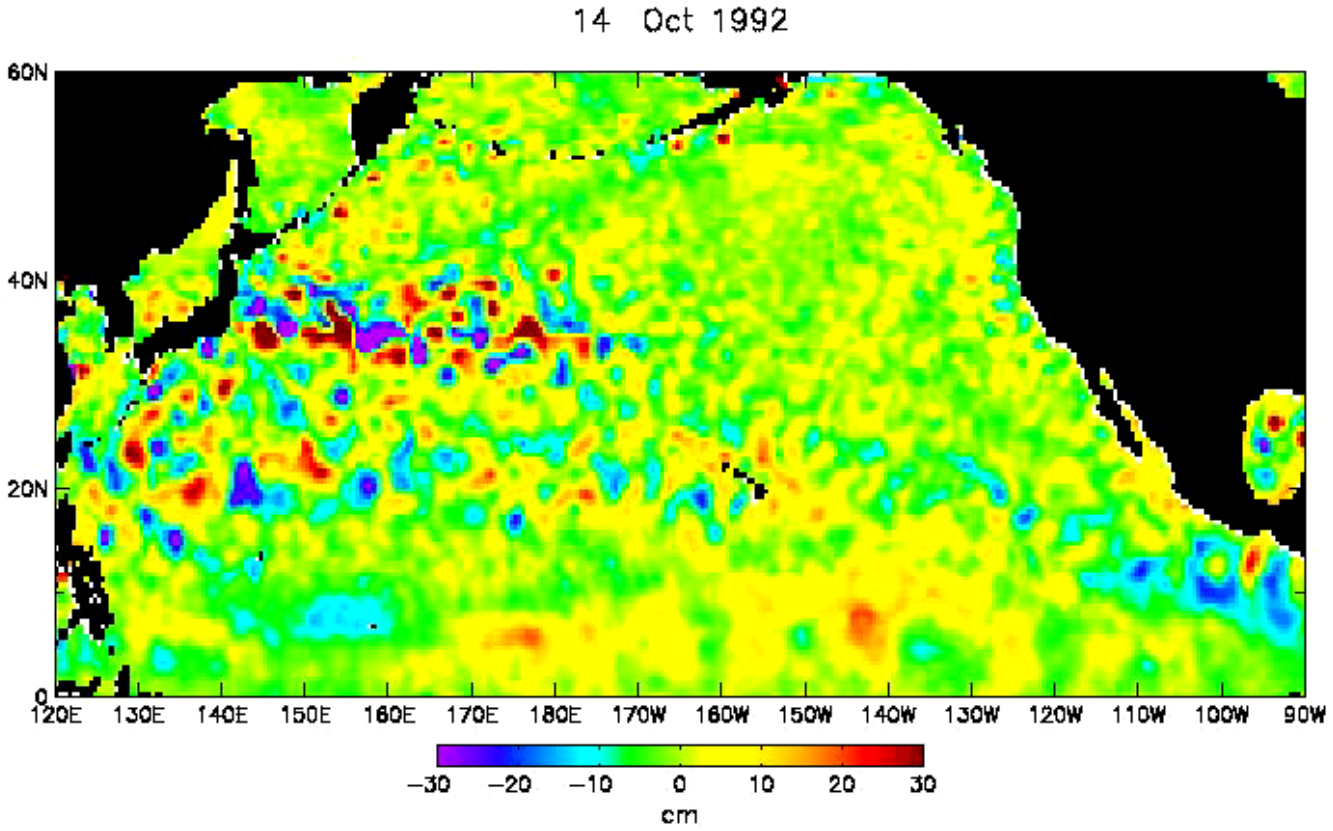

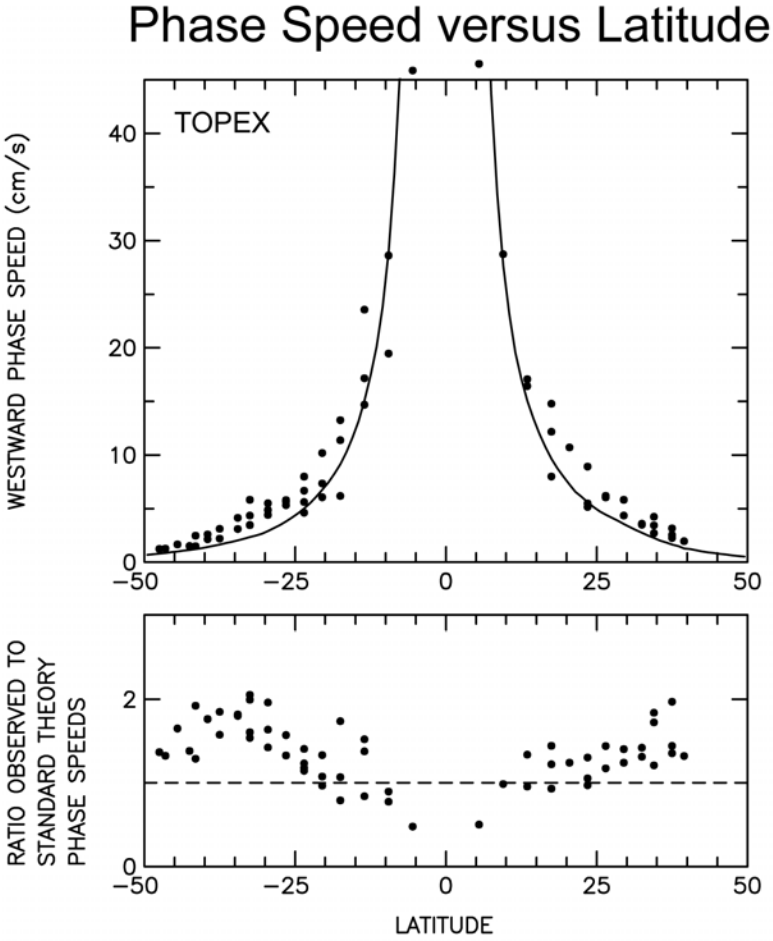


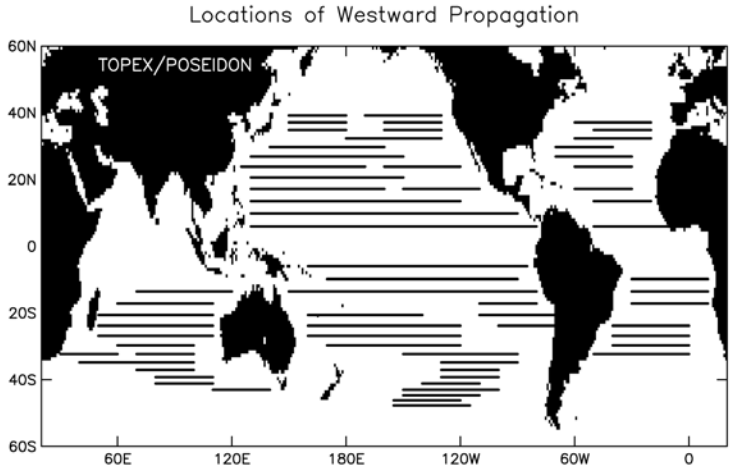


### Classical Theory

The dispersion relation from the classical theory for Rossby waves in the absence of any background mean current is

$$c_n \equiv \frac{\omega_n}{k} = \frac{-\beta}{k^2 + l^2 + \lambda_n^{-2}}$$

where $\lambda_n$ is the Rossby radius of deformation for the $n$th mode, which is determined by the buoyancy frequency profile $N(z)$ from the eigenvalue equation

$$\frac{d}{dz}\left(\frac{f_0^2}{N^2}\,\frac{d\phi_n}{dz}\right) + \frac{1}{\lambda_n^2}\,\phi_n = 0\,.$$

In the nondispersive (long-wave) limit of $k = l = 0$, this becomes

$$c_n = -\beta\lambda_n^2$$

The theoretical zonal phase speed $c_n$ is slower than this for nonzero $k$ or $l$.

# SSH Eddy Tracking Animation

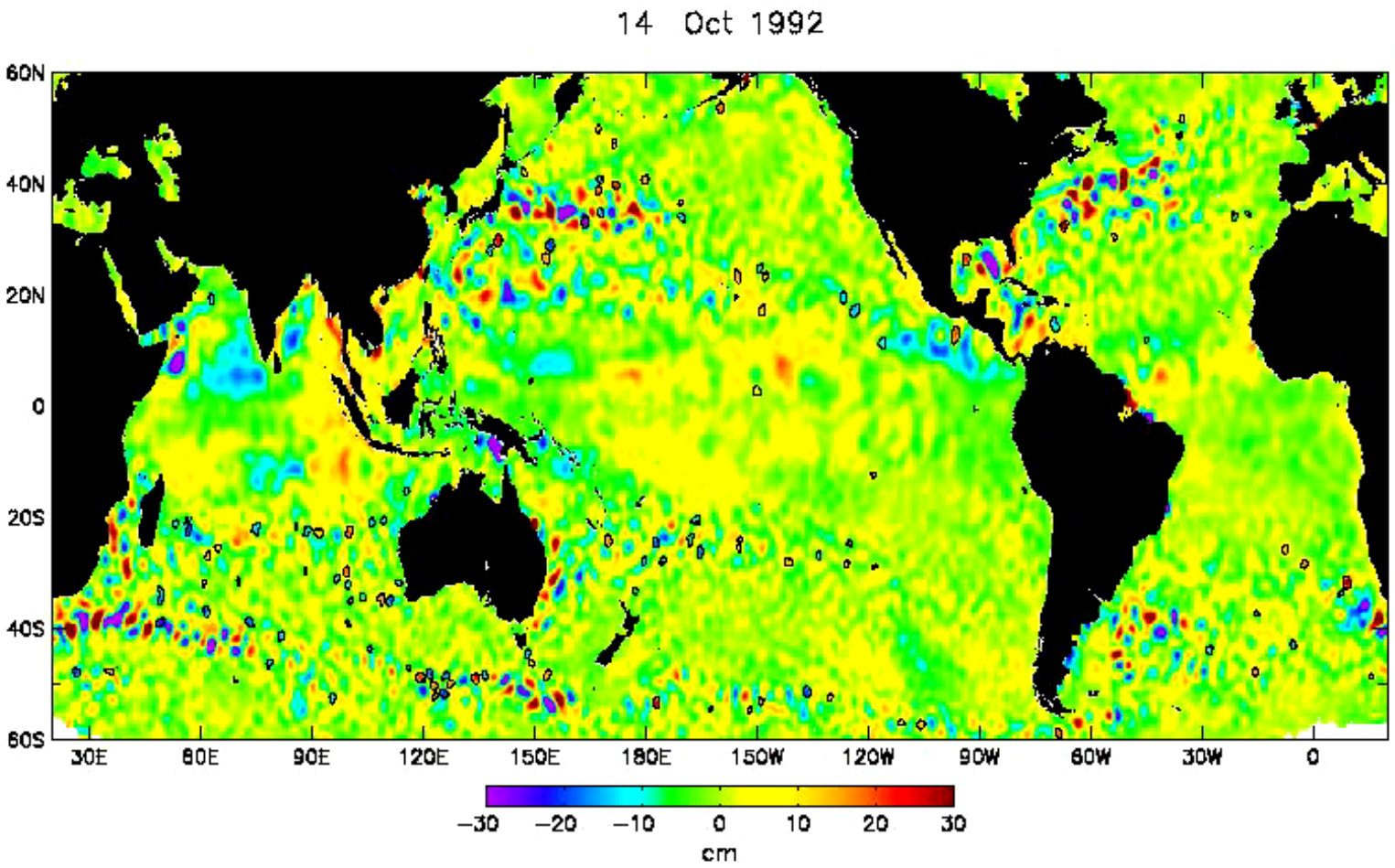

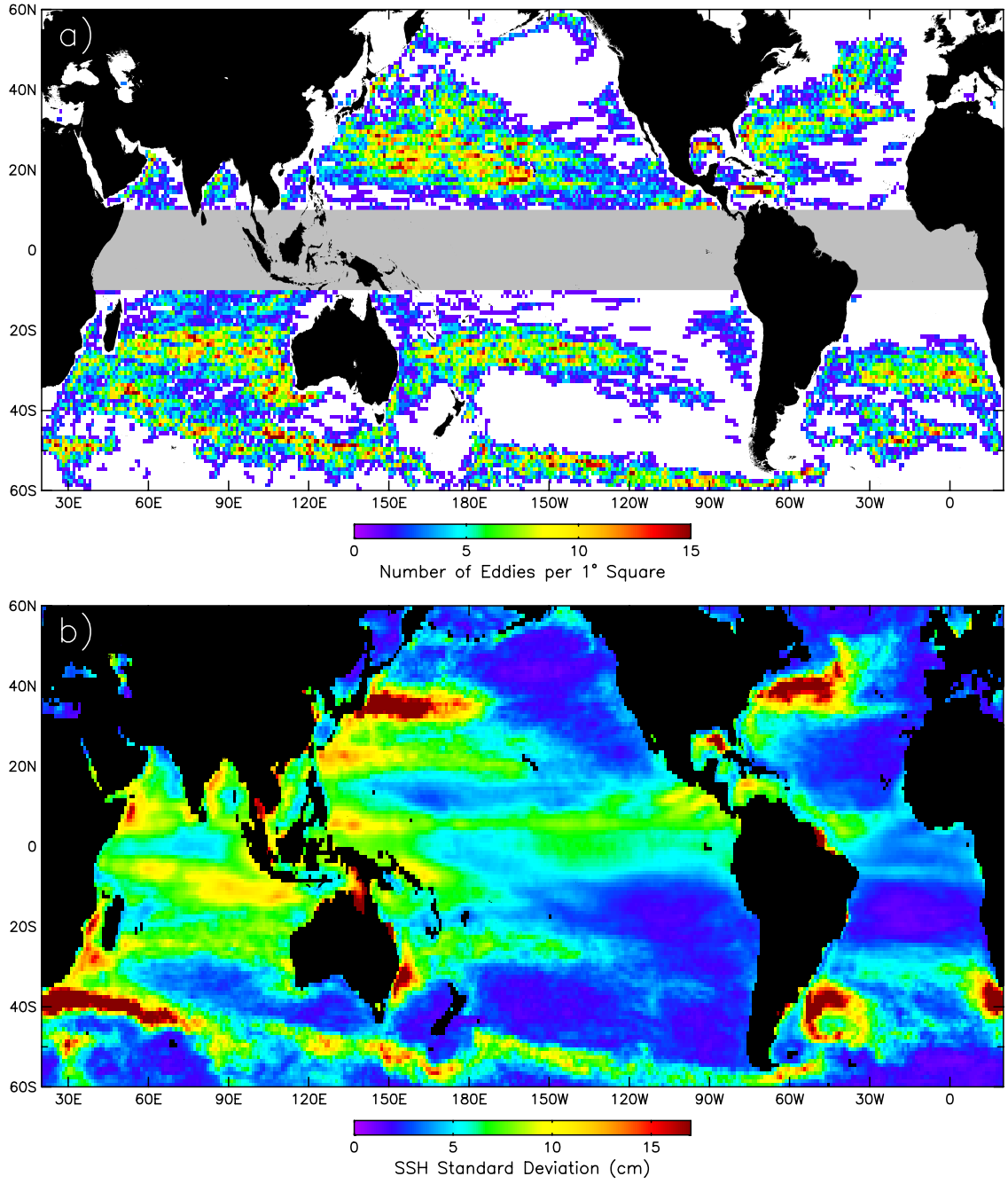
a)
60N
40N
20N
0
20S
40S
60S
30E
60E
90E
120E
150E
180E
150W
120W
90W
60W
30W
0
0
5
10
15
Number of Eddies per 1° Square
b)
60N
40N
20N
0
20S
40S
60S
30E
60E
90E
120E
150E
180E
150W
120W
90W
60W
30W
0
0
5
10
15
SSH Standard Deviation (cm)

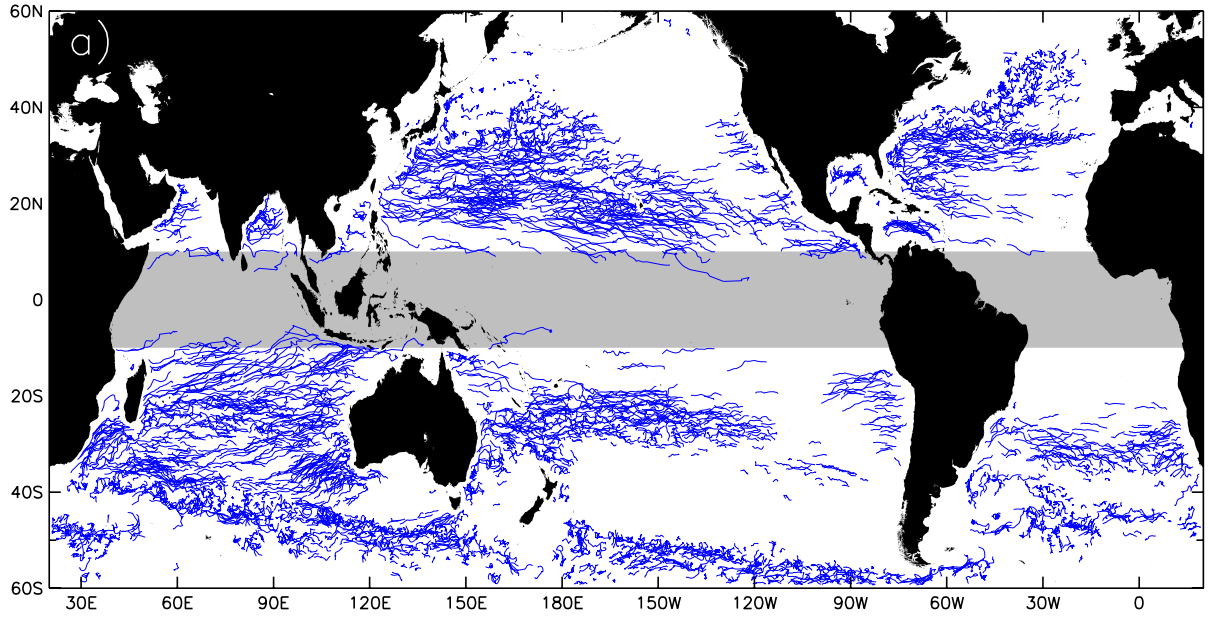


Cyclonic Eddy Trajectories (>18 Week Lifetimes)

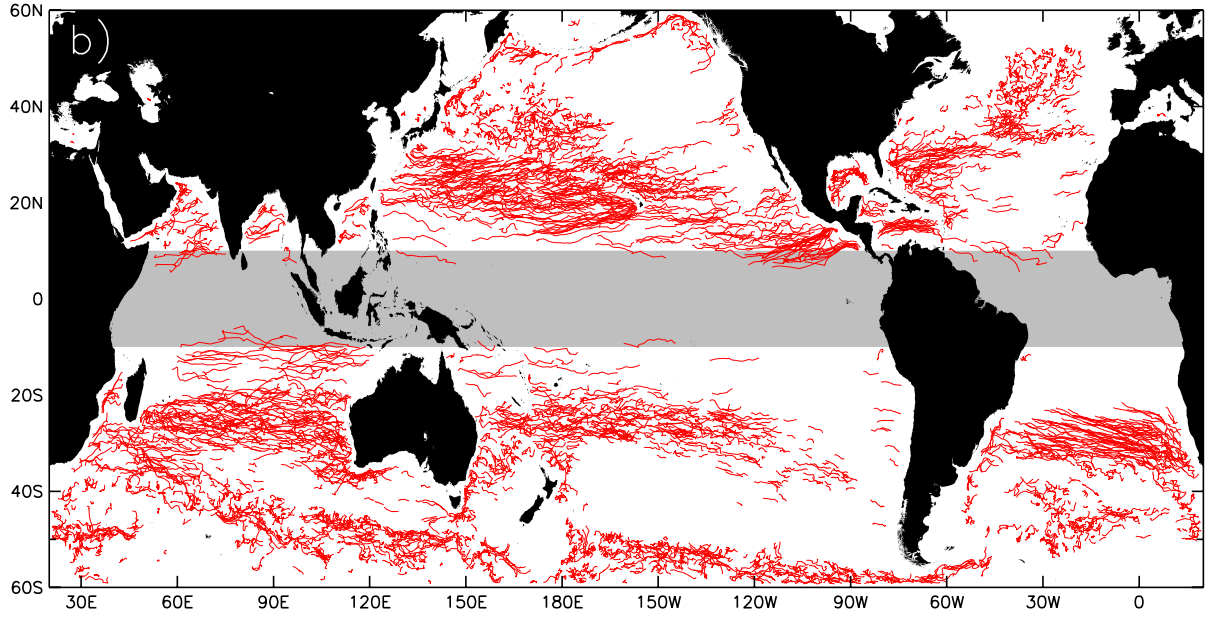


Anticyclonic Eddy Trajectories (>18 Week Lifetimes)

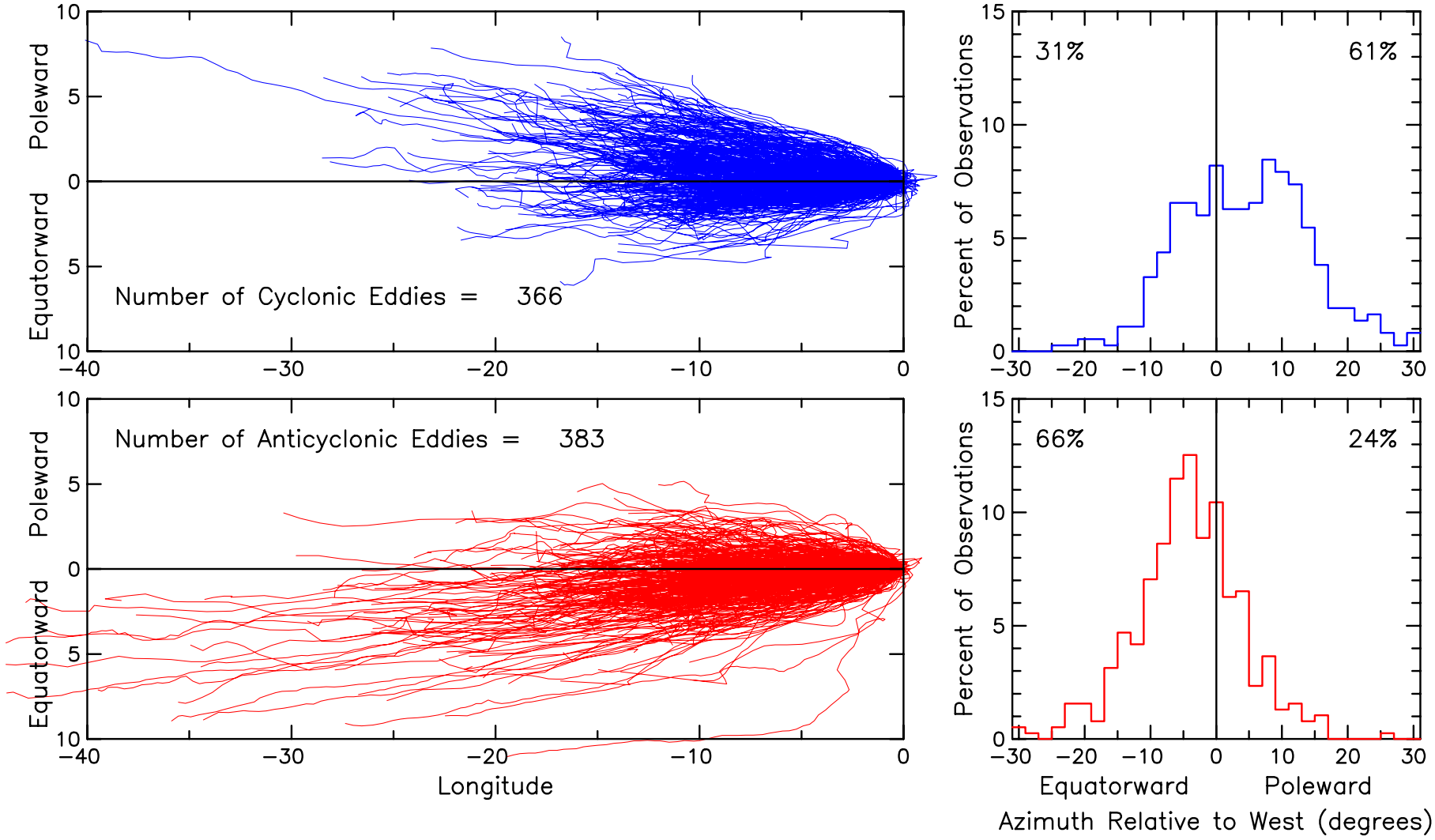
Poleward
Equatorward
Number of Cyclonic Eddies = 366
Number of Anticyclonic Eddies = 383
Longitude
Percent of Observations
31%
61%
66%
24%
Equatorward
Poleward
Azimuth Relative to West (degrees)

# Radar Scatterometry

NSCAT Launch

August 17, 1996
Tanegashima, Japan

QuikSCAT Launch

June 19, 1999
Vandenberg, California

# Radar Scatterometry

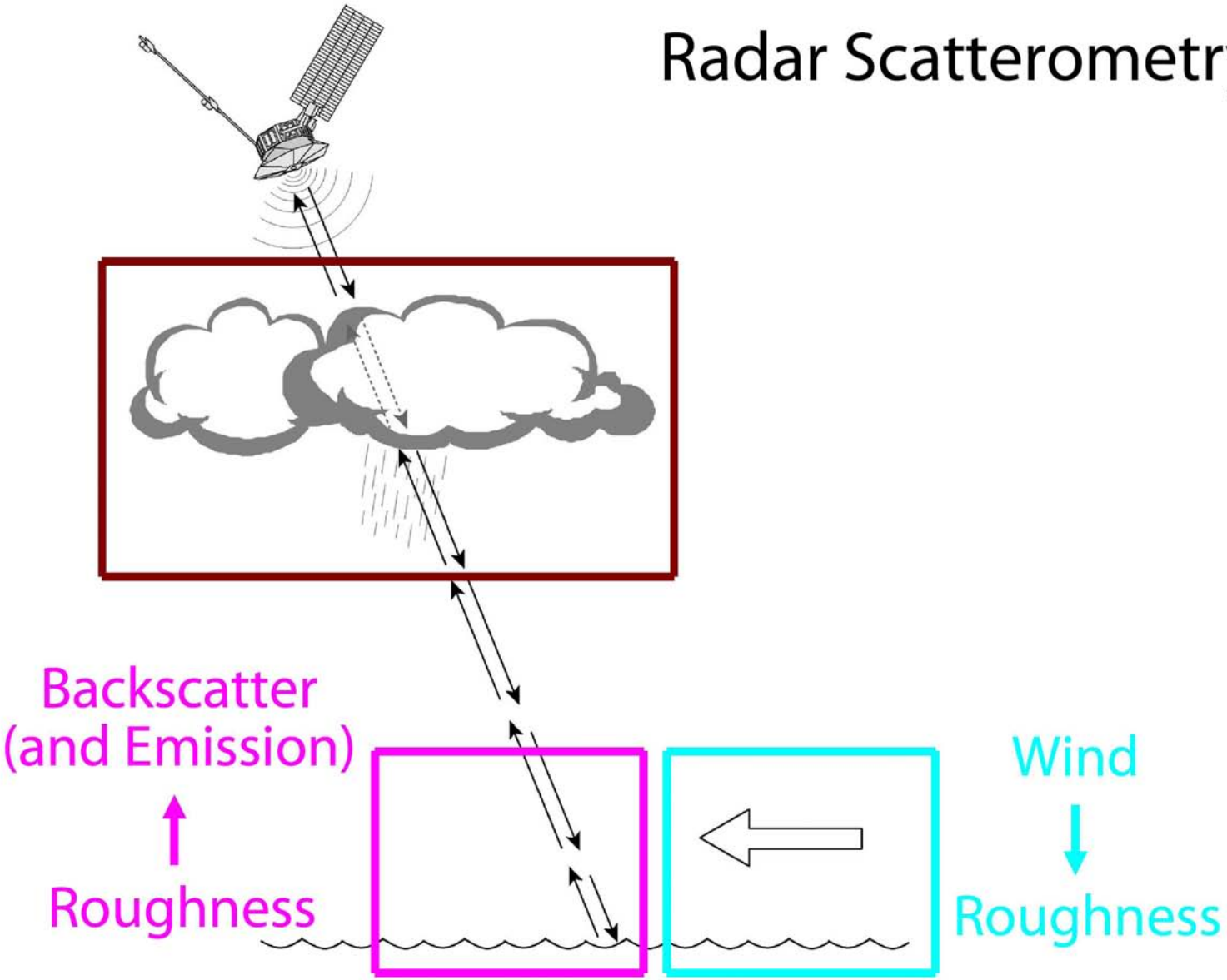


Figure courtesy of M. Freilich

# Bragg Scattering of the Radar Signal from Small-Scale Roughness on the Sea Surface

Resonant Bragg Scattering from Wavelengths Approximately Equal to that of the Radar Signal (~2 cm for a scatterometer frequency of 13.5 GHz)

$$\lambda_B = \frac{n}{2}\frac{\lambda}{\sin\theta}$$

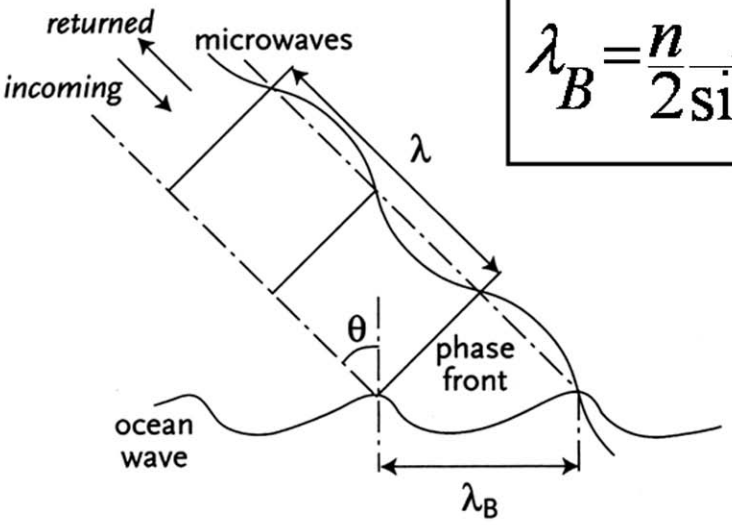


**Figure 11.** Bragg scattering: A plan-parallel radar beam with wavelength $\lambda$ hits the rough ocean surface at incidence angle $\theta$, where capillary gravity waves with Bragg wavelength $\lambda_B$ will cause microwave resonance.

Figure courtesy of A. Stoffelen

Centimetric Roughness: Gravity-Capillary Waves

Figure courtesy of M. Freilich

# Wind Speed and Direction Retrievals from Multiple Antenna Viewing Angles

The loci of possible solutions are at the intersections of the quasi-sinusoidal solutions from the multiple antenna viewing angles.

- *with only 2 viewing angles, there are typically 4 possible solutions for wind direction, all of which have about the same wind speed.*
- *with 4 viewing angles, the number of ambiguities in wind direction is usually reduced to only two, which differ by about 180° and have about the same speed. The 180° ambiguity is removed with a median filter algorithm that uses NCEP wind fields as a loosely constrained first guess.*

Solutions for 2 Antenna Viewing Angles

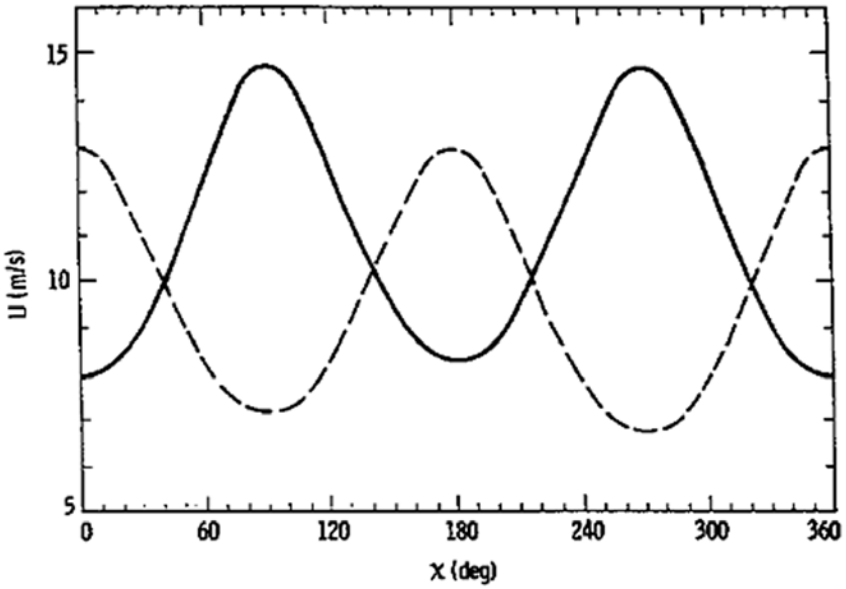


Solutions for 4 Antenna Viewing Angles

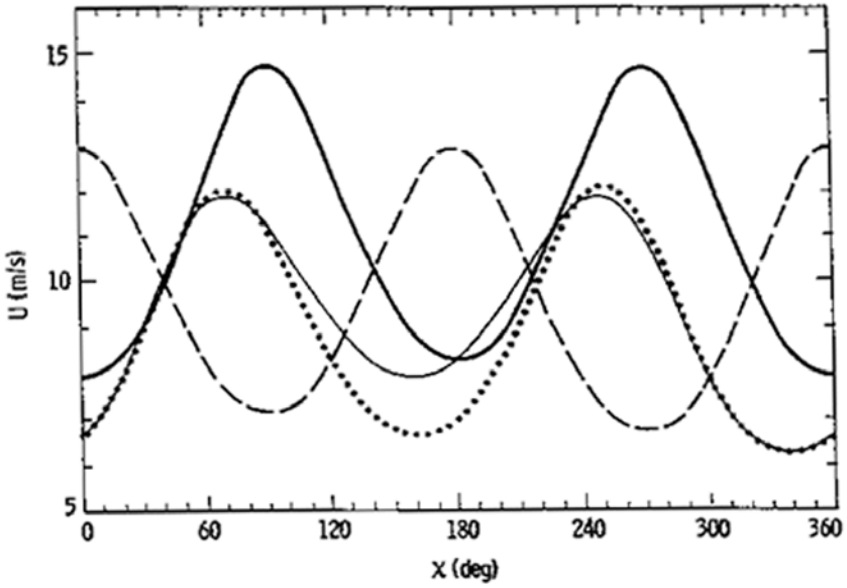


Figures courtesy of M. Freilich

# QuikSCAT Measurement Accuracy

Scatter Plot Comparisons Between NDBC Buoy Winds and Both NSCAT (thin lines) and QuikSCAT (heavy lines)

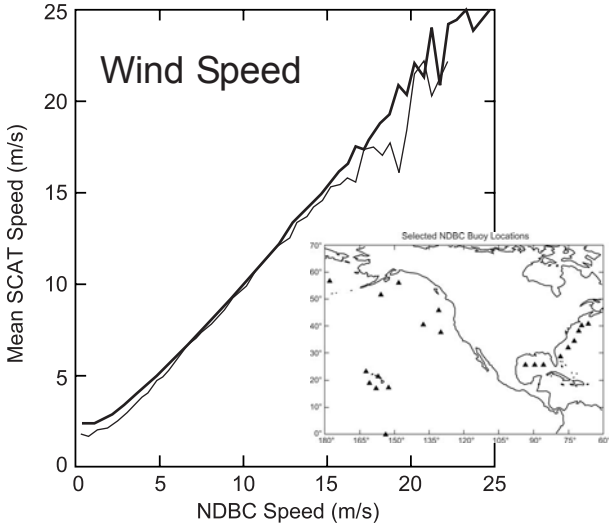


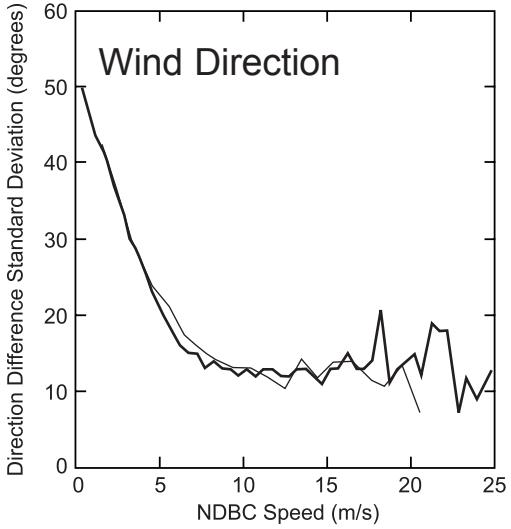


Standard Deviation of the Differences Between QuikSCAT and NCEP as a Function of Cross-Track Location

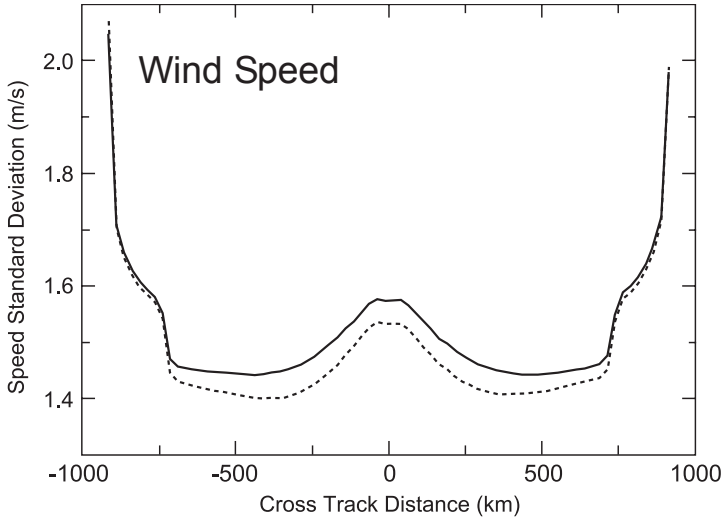


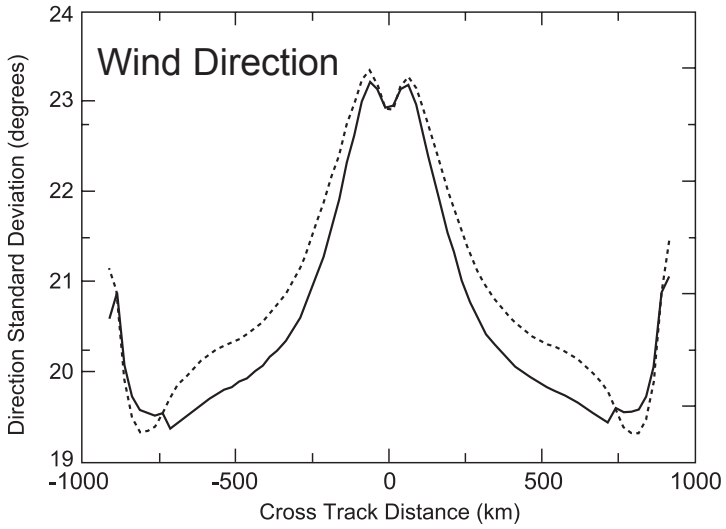

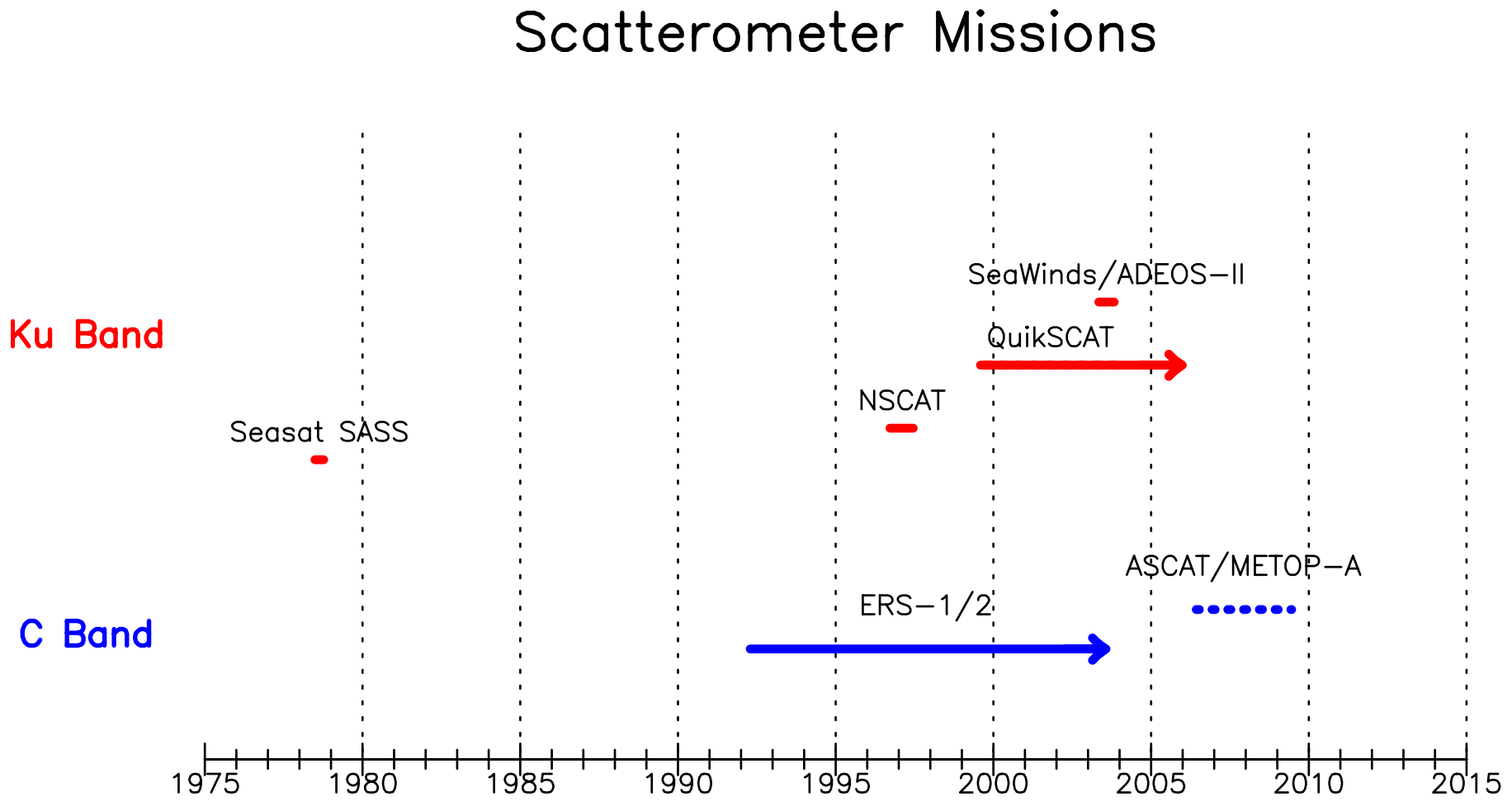
Scatterometer Missions
Ku Band
C Band
SeaWinds/ADEOS–II
QuikSCAT
NSCAT
Seasat SASS
ASCAT/METOP–A
ERS–1/2
1975
1980
1985
1990
1995
2000
2005
2010
2015

# Comparisons of QuikSCAT Wind Fields with ECMWF and NCEP Wind Fields

## Hurricane-Force Extratropical Cyclone in the North Pacific

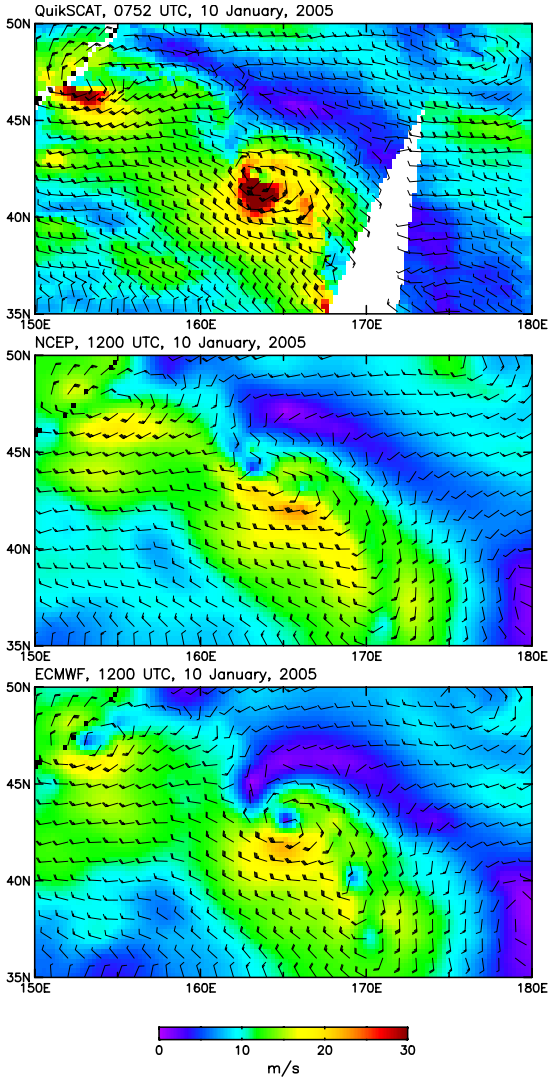


## SST-Induced Structure in the Wind Field over the Gulf Stream

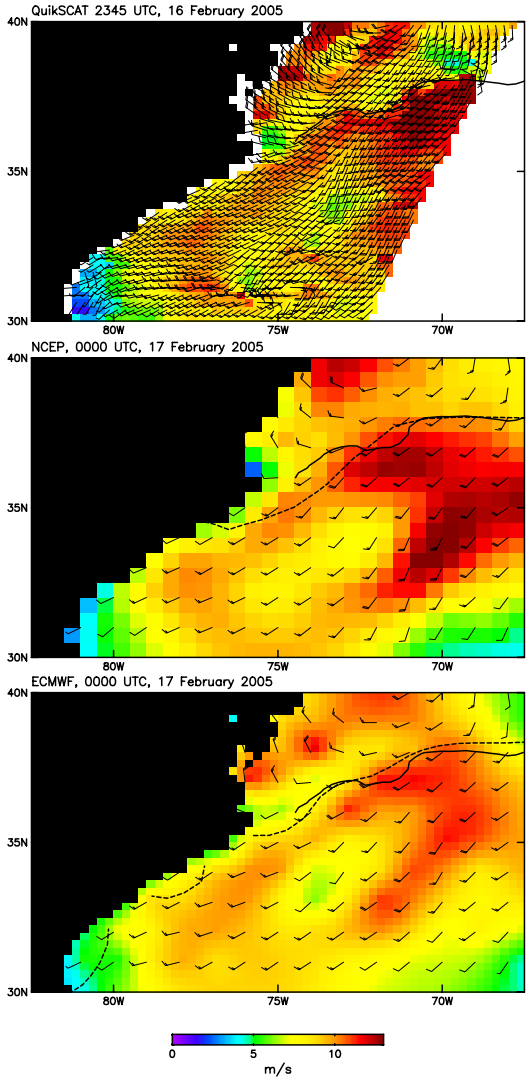

# Wind Shadow Behind the Galapagos Islands

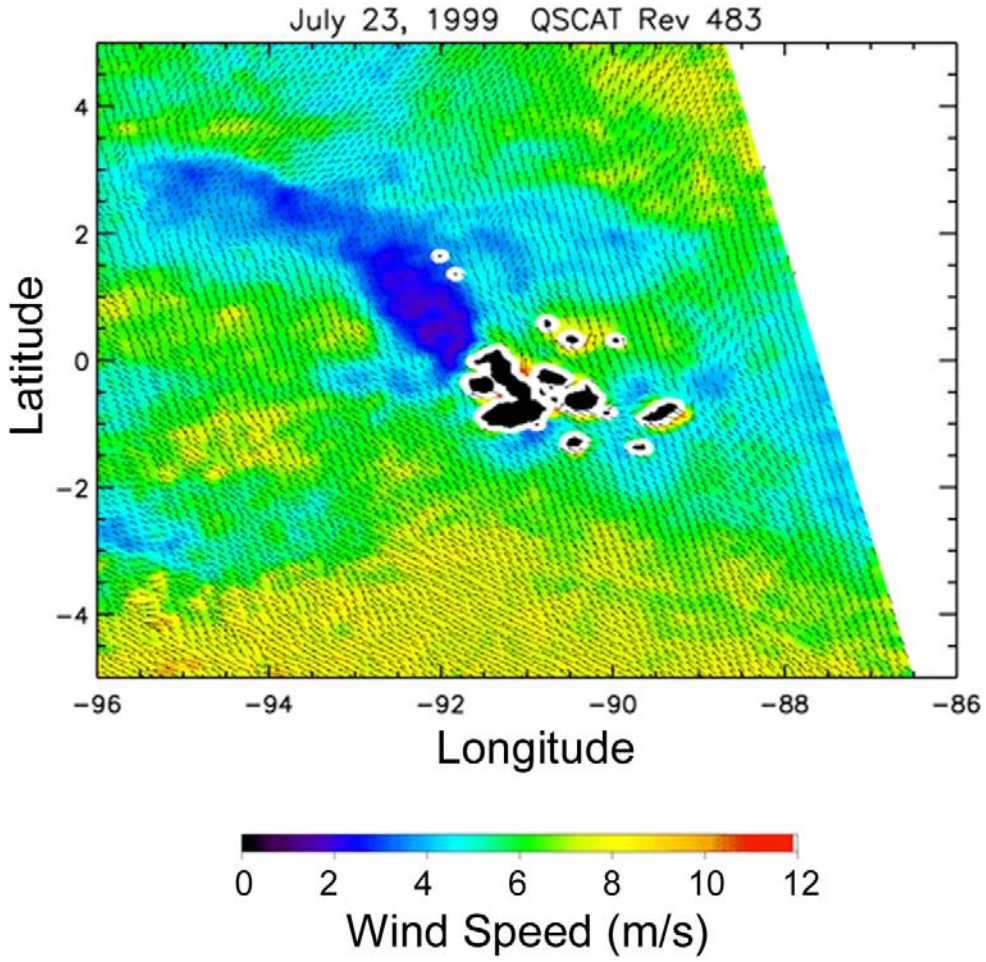


Figure courtesy of M. Freilich

# Wind Shadows Behind South Georgia Island

## NSCAT Example

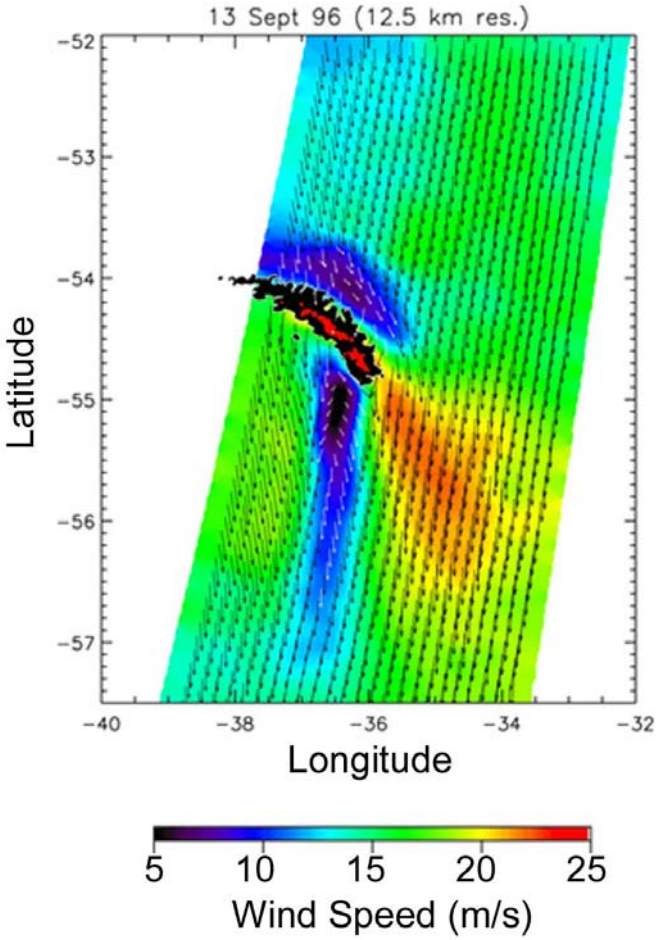


## QuikSCAT Example

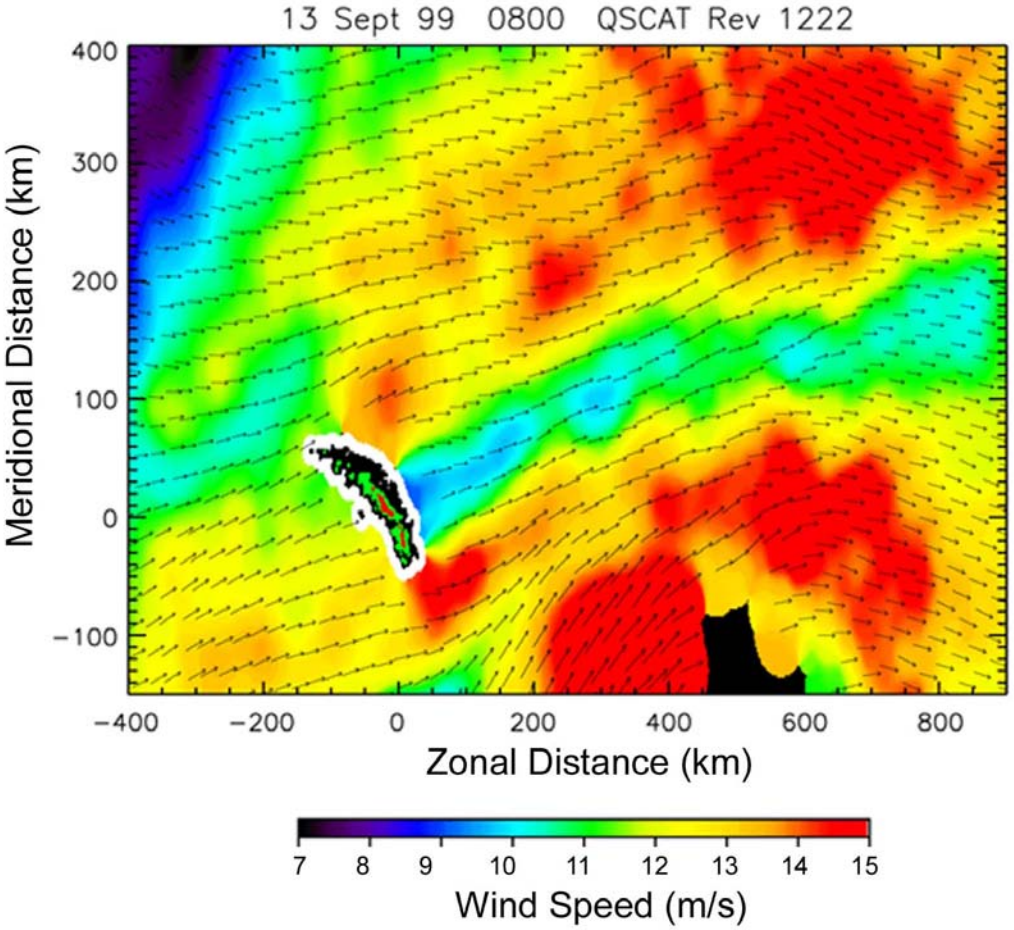


Figures courtesy of M. Freilich

# Flow Distortion by Orographic Effects as Evidenced in the Wind Stress Curl (Wind Jets and Wind Shadows)

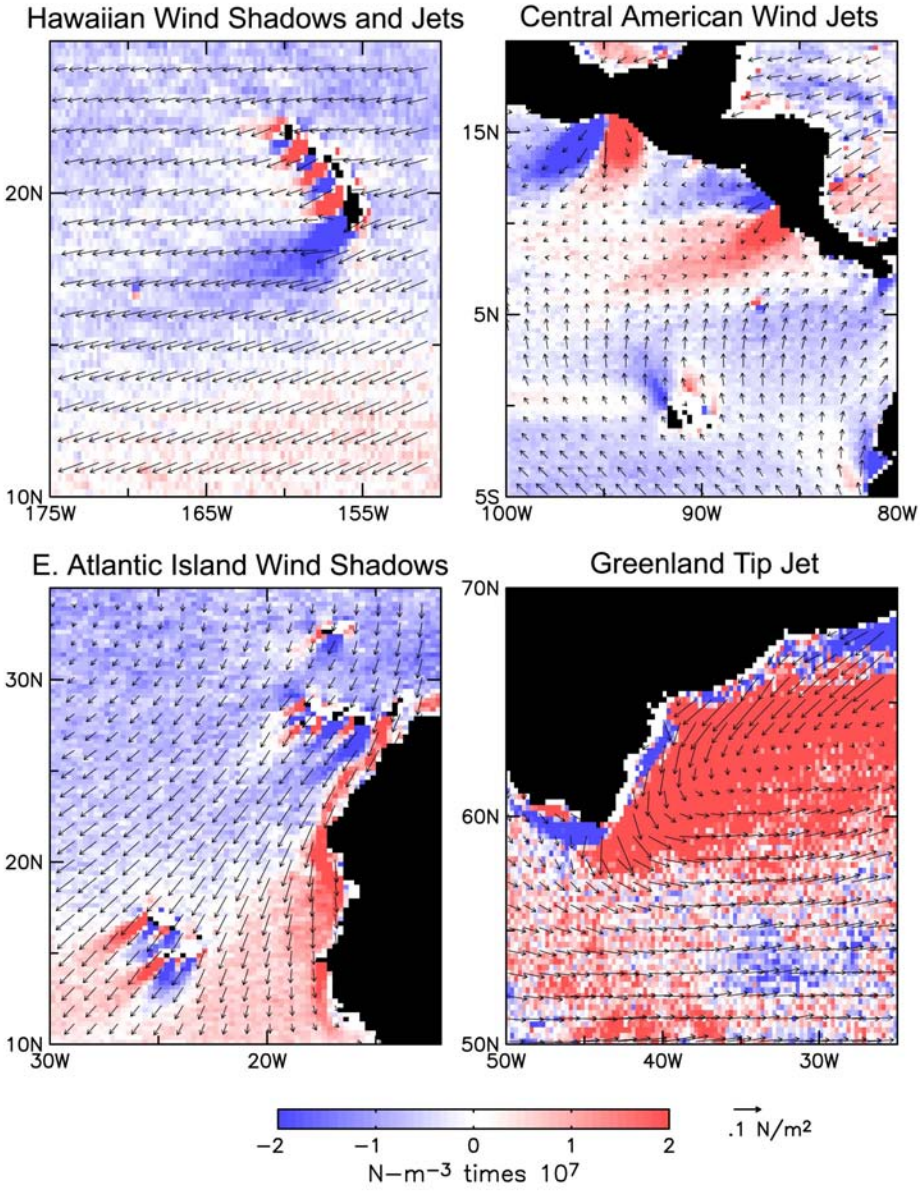

# 2-Month Average Wind Stress Magnitude

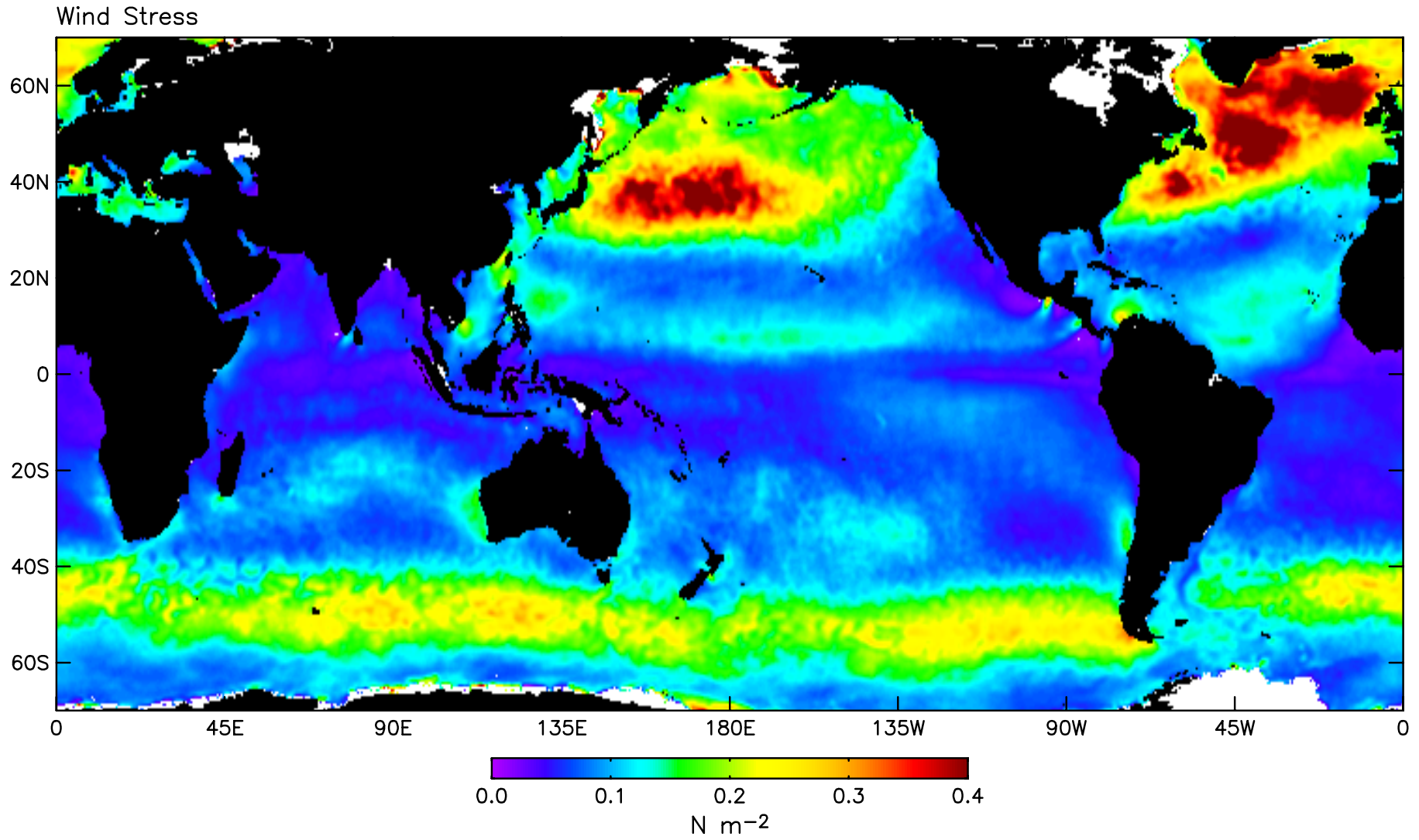

# 2-Month Average Wind Stress Magnitude

## (Spatially High-Pass Filtered)

QuikSCAT, January–February 2003

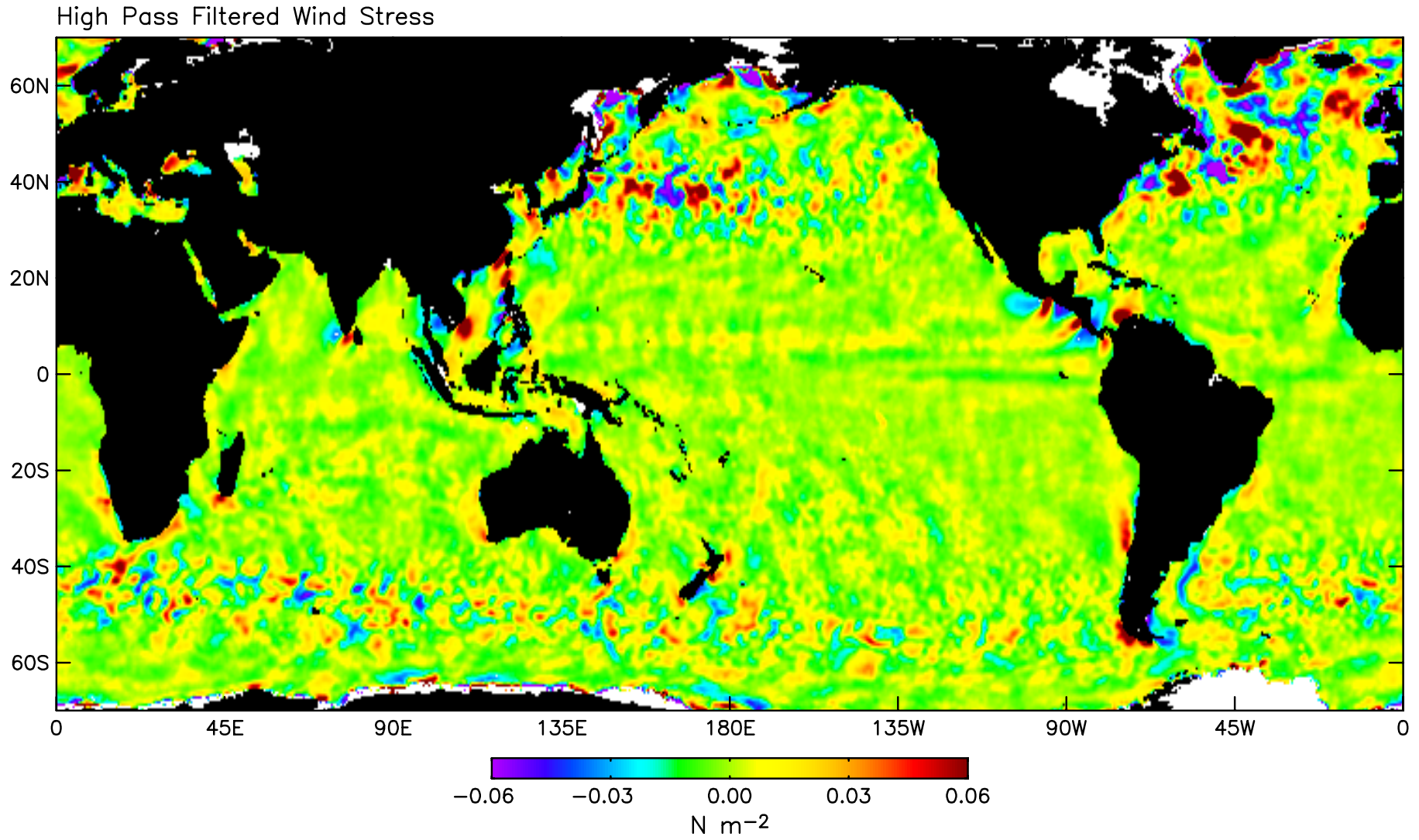

# 2-Month Average Wind Stress Magnitude and SST

## (Spatially High-Pass Filtered)

QuikSCAT, January–February 2003

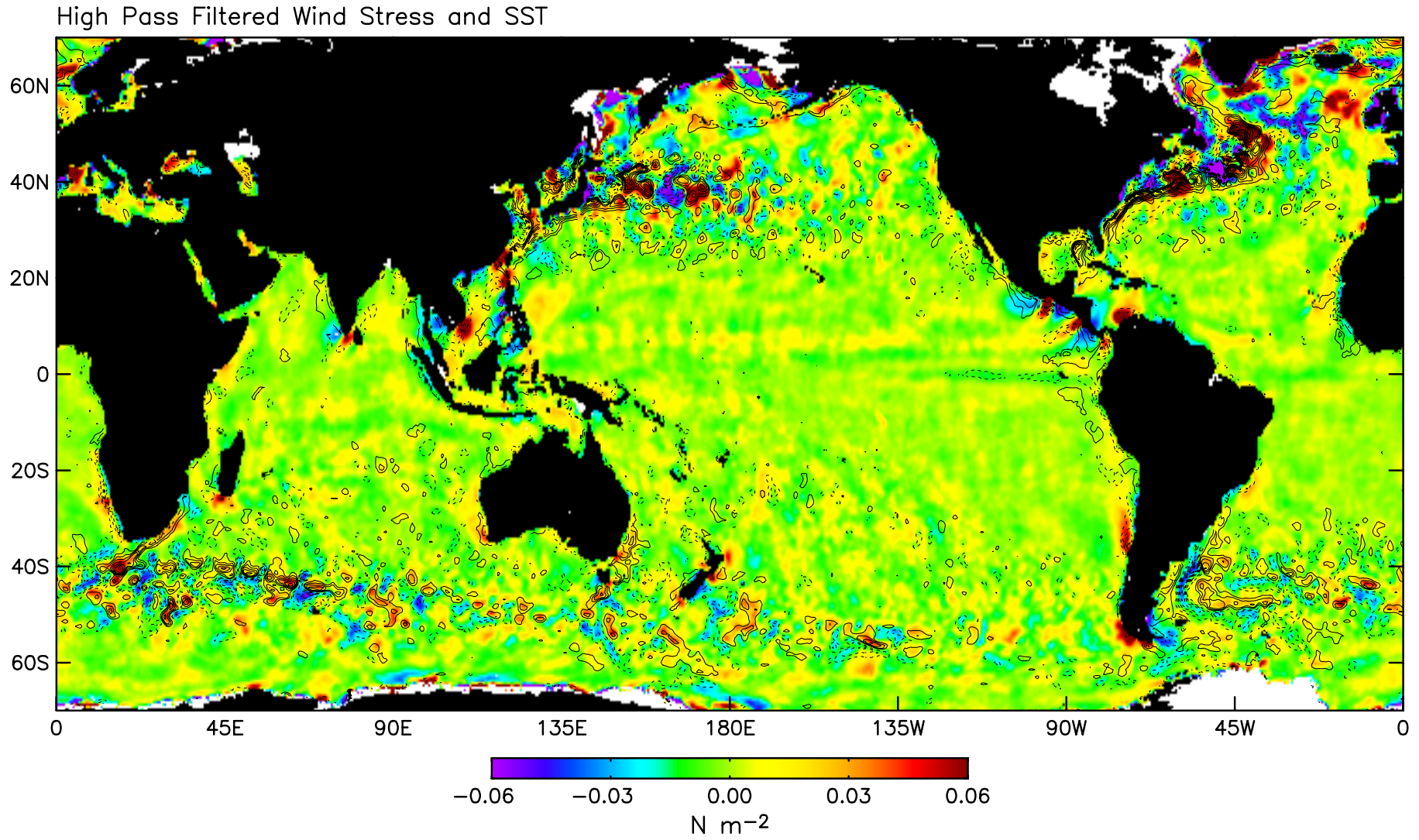

# High-Resolution Spatially High-Pass Filtered SST from AMSR and Wind Speed from QuikSCAT

July 2002 - February 2003 Average

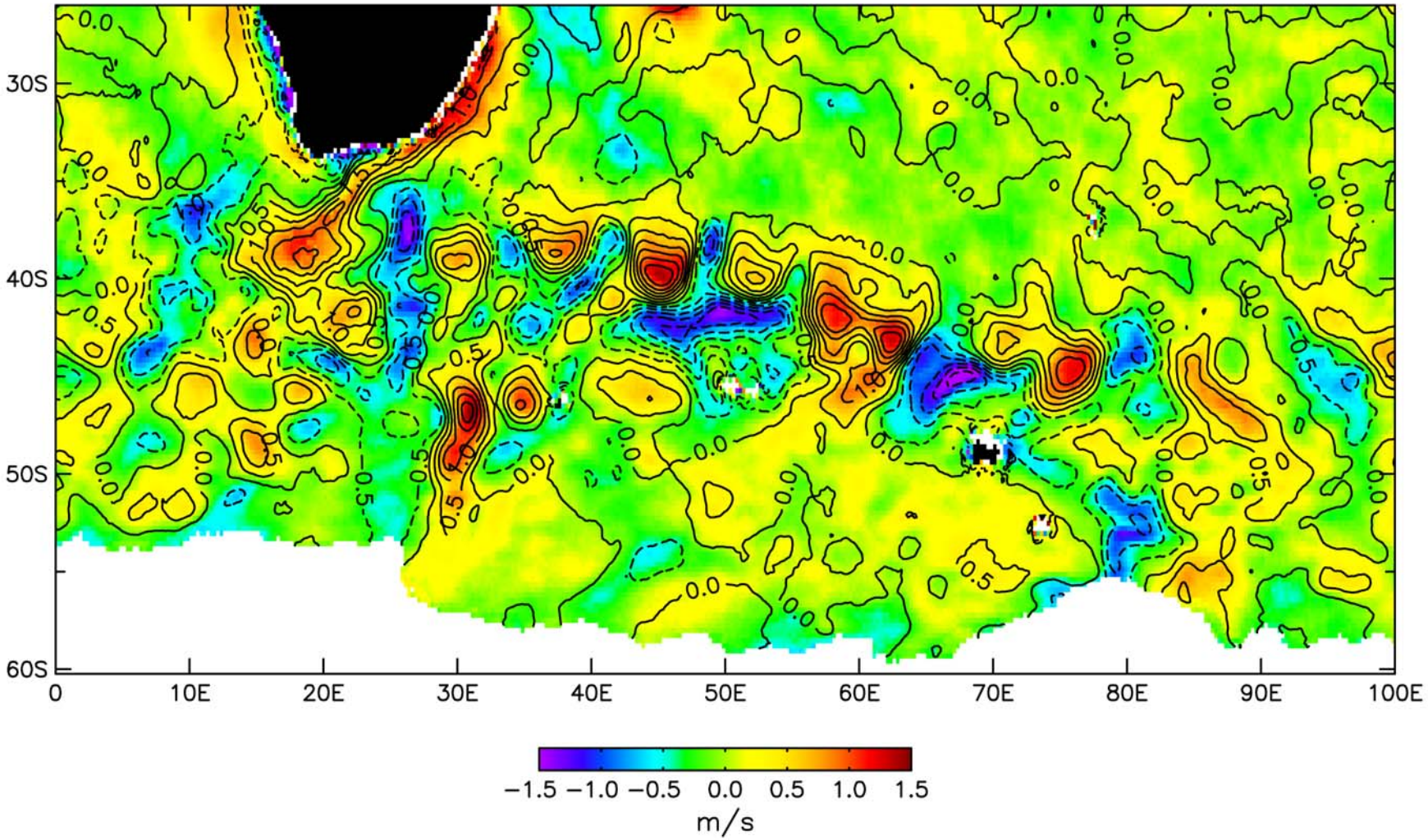

# Wind Stress Vectors and SST, 12 December 2001

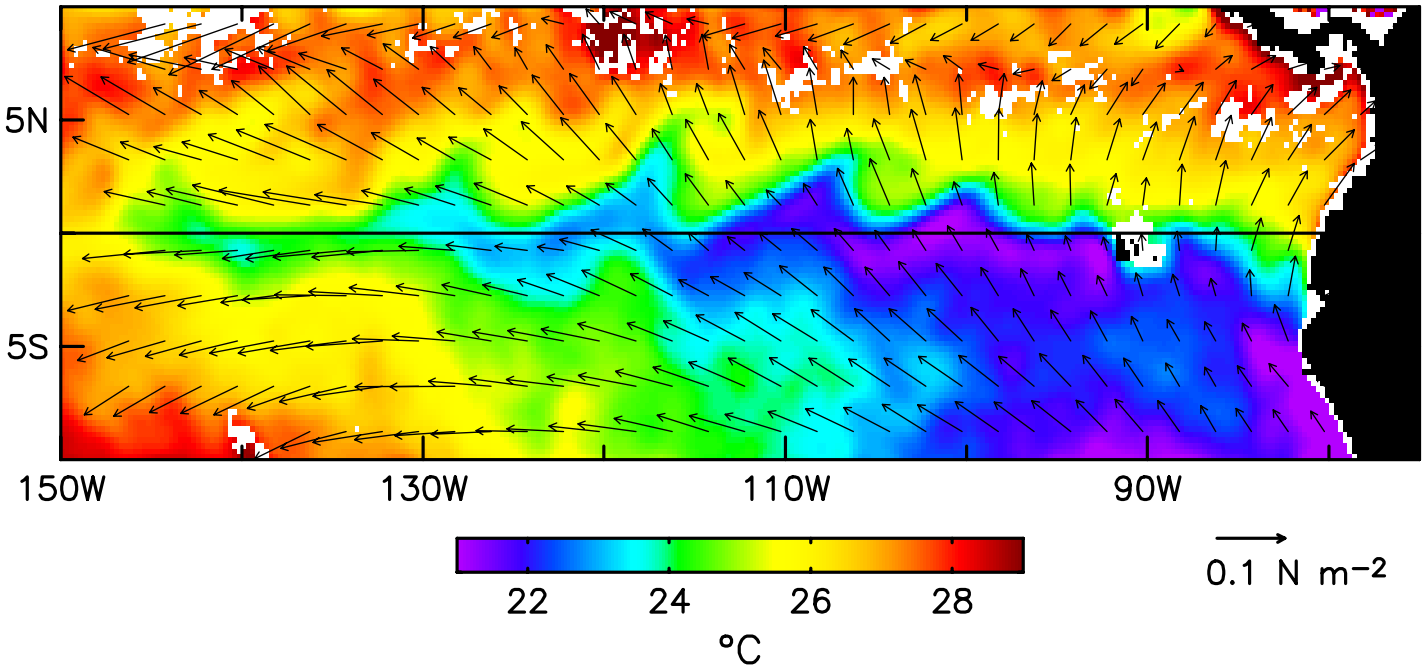


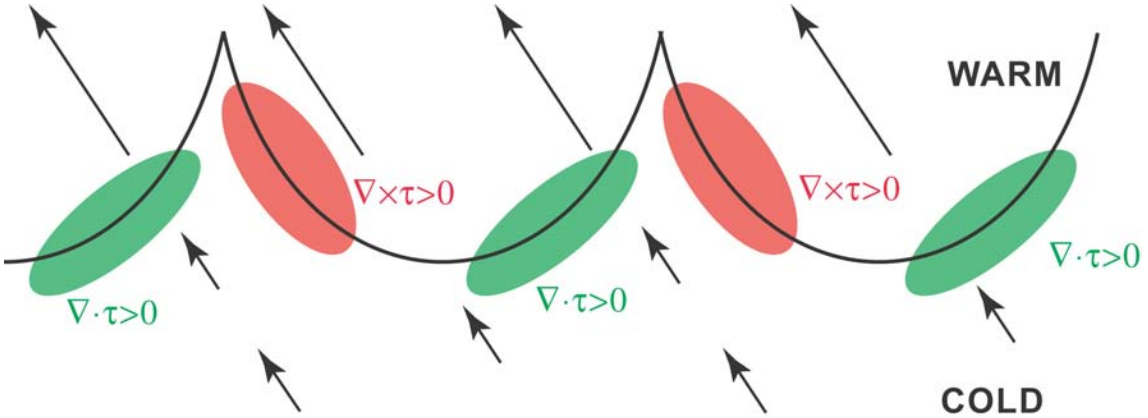

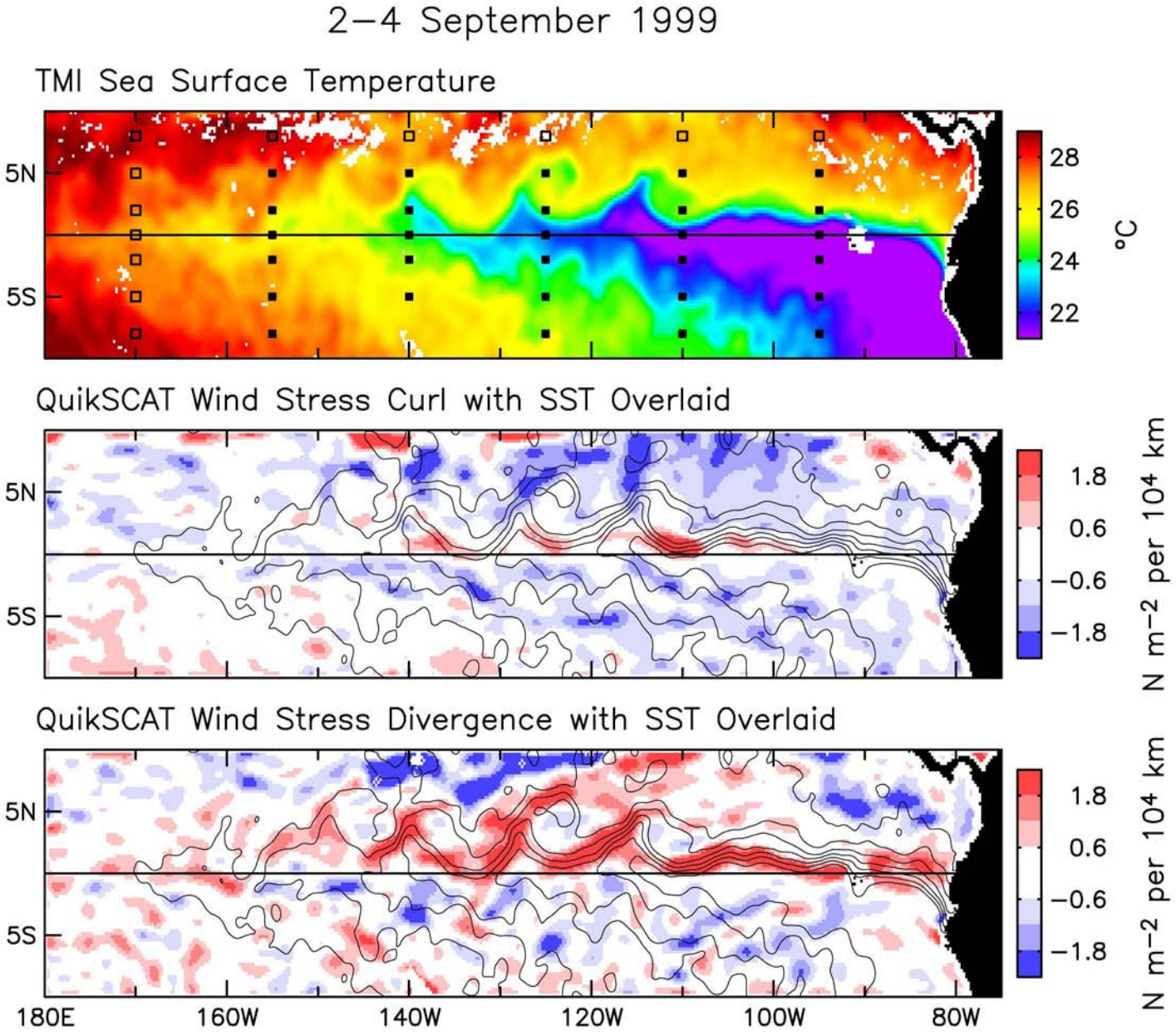
2–4 September 1999
TMI Sea Surface Temperature
5N
5S
28
26
24
22
°C
QuikSCAT Wind Stress Curl with SST Overlaid
5N
5S
1.8
0.6
−0.6
−1.8
N m−2 per 104 km
QuikSCAT Wind Stress Divergence with SST Overlaid
5N
5S
1.8
0.6
−0.6
−1.8
N m−2 per 104 km
180E
160W
140W
120W
100W
80W

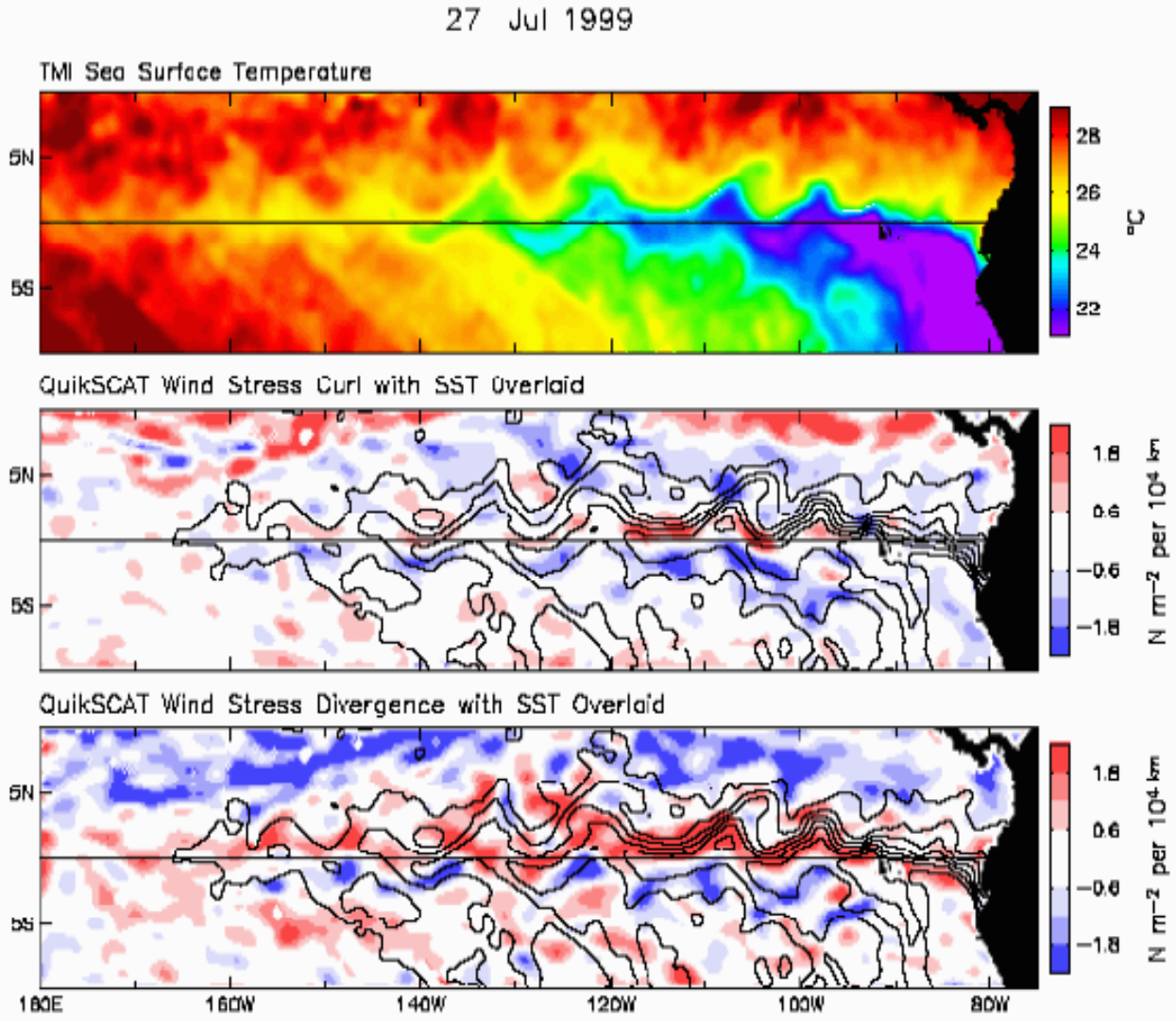
27 Jul 1999
TMI Sea Surface Temperature
5N
5S
28
26
24
22
°C
QuikSCAT Wind Stress Curl with SST Overlaid
5N
5S
1.8
0.6
−0.6
−1.8
N m−2 per 10^4 km
QuikSCAT Wind Stress Divergence with SST Overlaid
5N
5S
1.8
0.6
−0.6
−1.8
N m−2 per 10^4 km
180E
160W
140W
120W
100W
80W

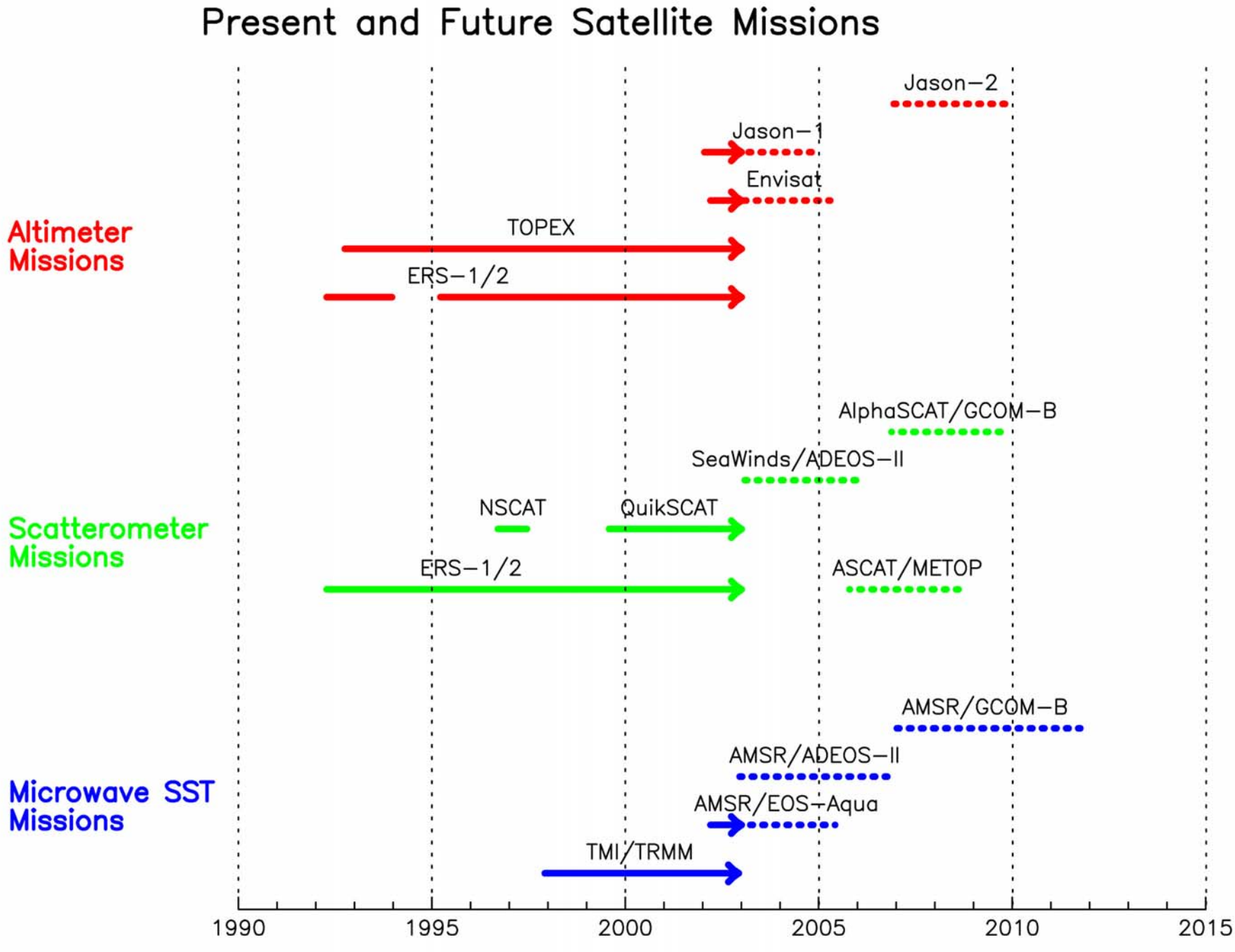
Present and Future Satellite Missions
Altimeter Missions
Scatterometer Missions
Microwave SST Missions
Jason−2
Jason−1
Envisat
TOPEX
ERS−1/2
AlphaSCAT/GCOM−B
SeaWinds/ADEOS−II
NSCAT
QuikSCAT
ERS−1/2
ASCAT/METOP
AMSR/GCOM−B
AMSR/ADEOS−II
AMSR/EOS−Aqua
TMI/TRMM
1990
1995
2000
2005
2010
2015

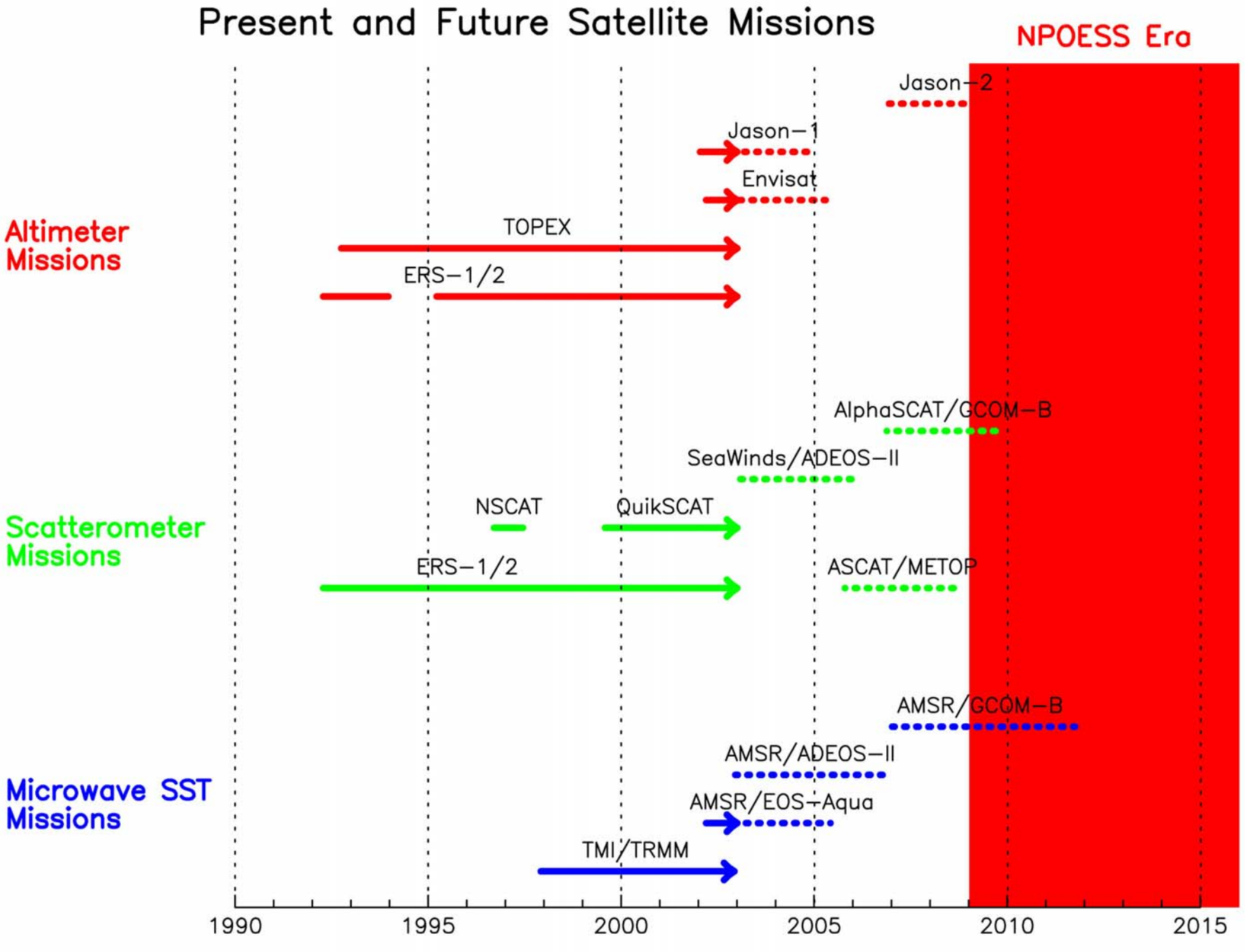
Present and Future Satellite Missions
NPOESS Era
Jason−2
Jason−1
Envisat
Altimeter Missions
TOPEX
ERS−1/2
AlphaSCAT/GCOM−B
SeaWinds/ADEOS−II
NSCAT
QuikSCAT
Scatterometer Missions
ERS−1/2
ASCAT/METOP
AMSR/GCOM−B
AMSR/ADEOS−II
AMSR/EOS−Aqua
Microwave SST Missions
TMI/TRMM
1990
1995
2000
2005
2010
2015

# Challenge for the Future:

*Sustaining continuous records of high-quality satellite observations for climate research.*

- Climate time scales are much longer than individual satellite missions.
- Satellite observations for ocean climate studies must therefore be acquired from operational satellite programs. (NPOESS???)
- The links between the oceans research community and the various national space agencies must be strengthened to assure the quality and long-term continuity of satellite observations.
- These links must be formalized soon...the time from conception to launch of a satellite instrument is about 10 years.